





# SLC35B2 Acts in a Dual Role in the Host Sulfation Required for EV71 Infection

Dong Guo,<sup>a</sup> Xinghai Yu,<sup>a</sup> Dan Wang,<sup>a</sup> Zhifei Li,<sup>a</sup>  Yu Zhou,<sup>a</sup> Guodong Xu,<sup>b</sup> Bing Yuan,<sup>b</sup> Yali Qin,<sup>a</sup>  Mingzhou Chen<sup>a</sup>

<sup>a</sup>State Key Laboratory of Virology and Modern Virology Research Center, College of Life Sciences, Wuhan University, Wuhan, China

<sup>b</sup>Wuhan Canvest Biotechnology Co., Ltd., Wuhan, Hubei, China

**ABSTRACT** As an important neurotropic enterovirus, enterovirus 71 (EV71) is occasionally associated with severe neurological diseases and high mortality rates in infants and young children. Understanding the interaction between host factors and EV71 will play a vital role in developing antivirals and optimizing vaccines. Here, we performed a genome-wide CRISPR-Cas9 knockout screen and revealed that scavenger receptor class B member 2 (SCARB2), solute carrier family 35 member B2 (SLC35B2), and beta-1,3-glucuronyltransferase 3 (B3GAT3) are essential in facilitating EV71 replication. Subsequently, the exploration of molecular mechanisms suggested that the knockout of SLC35B2 or B3GAT3, not SCARB2, led to a remarkable decrease in the binding of EV71 to cells and internalization into cells. Furthermore, we found that the infection efficiency for EV71 was positively correlated with the level of host cell sulfation, not simply with the amount of heparan sulfate, suggesting that an unidentified sulfated protein(s) must contribute to EV71 infection. In support of this idea, we screened possible sulfated proteins among the proteinous receptors for EV71 and confirmed that SCARB2 could uniquely interact with both tyrosyl protein sulfotransferases in humans. We then performed mass spectrometric analysis of SCARB2, identifying five sites with tyrosine sulfation. The function verification test indicated that there were more than five tyrosine-sulfated sites on SCARB2. Finally, we constructed a model for EV71 entry in which both heparan sulfate and SCARB2 are regulated by SLC35B2 and act cooperatively to support viral binding, internalization, and uncoating. Taken together, this is the first time that we performed the pooled CRISPR-Cas9 genetic screening to investigate the interplay of host cells and EV71. Furthermore, we found that a novel host factor, SLC35B2, played a dual role in regulating the overall sulfation comprising heparan sulfate sulfation and protein tyrosine sulfation, which are critical for EV71 entry.

**IMPORTANCE** As the most important nonpolio neurotropic enterovirus lacking specific treatments, EV71 can transmit to the central nervous system, leading to severe and fatal neurological complications in infants and young children. The identification of new factors that facilitate or inhibit EV71 replication is crucial to uncover the mechanisms of viral infection and pathogenesis. To date, only a few host factors involved in EV71 infection have been characterized. Herein, we conducted a genome-wide CRISPR-Cas9 functional knockout (GeCKO) screen for the first time to study EV71 in HeLa cells. The screening results are presented as a ranked list of candidates, including 518 hits in the positive selection that facilitate EV71 replication and 1,044 hits in the negative selection that may be essential for cell growth and survival or for suppressing EV71 infection. We subsequently concentrated on the top three hits in the positive selection: SCARB2, SLC35B2, and B3GAT3. The knockout of any of these three genes confers strong resistance against EV71 infection. We confirmed that EV71 infection is codependent on two receptors, heparan sulfate and SCARB2. We also identified a host entry factor, SLC35B2, indirectly facilitating EV71 infection through regulation of the host cell sulfation, and determined a novel posttranslational modification, protein tyrosine sulfation existing in SCARB2. This study revealed that EV71 infectivity exhibits a significant positive correlation with the level of cellular sulfation regulated by SLC35B2.

**Editor** Bryan R. G. Williams, Hudson Institute of Medical Research

**Copyright** © 2022 American Society for Microbiology. All Rights Reserved.

Address correspondence to Yali Qin, yqin@whu.edu.cn, or Mingzhou Chen, chenmz@whu.edu.cn.

The authors declare no conflict of interest.

**Received** 26 November 2021

**Accepted** 22 March 2022

**Published** 14 April 2022

Due to the sulfation pathway being required for many distinct viruses, including but not limited to EV71 and respiratory syncytial virus (RSV), which were tested in this study, SLC35B2 represents a target of broad-spectrum antiviral therapy.

**KEYWORDS** CRISPR screening, enterovirus 71, host entry factor, tyrosine sulfation

Enterovirus 71 (EV71) is the second most common causative pathogen for hand, foot, and mouth disease (HFMD) after coxsackievirus A16 (CV-A16). As a neurotropic virus, EV71 can lead to severe neurological complications, which can cause death, including aseptic meningitis, acute brainstem encephalitis, acute flaccid paralysis, and neurogenic pulmonary edema associated with high mortality (1–3). The combination of specific antivirals with effective vaccines will accelerate the eradication of EV71. Therefore, it is necessary to intensively investigate EV71 to fully elucidate its life cycle and identify promising targets for broad-range antiviral drugs to make up for the limitations of these vaccines.

Generally, enteroviral receptors mediate the early steps of the viral life cycle, including the binding of EV71 to the cell surface, internalization of EV71 via endocytosis, and uncoating of viral RNA in the cytoplasm. To date, at least seven molecules have been identified as possible receptors for EV71, including only one well-characterized entry receptor, scavenger receptor class B2 (SCARB2) (4), and six attachment receptors: P-selectin glycoprotein ligand-1 (PSGL-1) (5), nucleolin (NCL) (6), annexin II (ANX2) (7), vimentin (VIM) (8), heparan sulfate proteoglycan (HSPG) (9), and sialylated glycan (10). Other molecules such as DC-SIGN (dendritic cell-specific intercellular adhesion molecule-3 grabbing nonintegrin) (11), prohibitin (12), and fibronectin (13) may play a similar role to the attachment receptor in stimulating EV71 infection. Given the multiple available receptors for EV71, it is important to evaluate or compare the infection efficiencies of EV71 via different receptors and investigate the individual roles and combined effects of these receptors during viral entry. These studies will help in understanding the pathogenicity of EV71 and developing possible strategies by which to prevent viral infection.

SCARB2 is widely expressed in a variety of cell lines, including human rhabdomyosarcoma (RD), HeLa, HEp-2, HEK293T, and HepG2 (4), and highly expressed in neurons, lung pneumocytes, hepatocytes, and some epithelia *in vivo* (14). At least 10 N-linked glycosylation sites for the human SCARB2 protein have been previously reported (15). Notably, SCARB2 is a sialylated glycoprotein, and the desialylation of SCARB2 abolishes the interaction between SCARB2 and EV71, implying that cell surface sialylation should be a critical regulator that facilitates the binding of EV71 to host cells and infection (16). SCARB2 is a receptor capable of facilitating viral attachment to the cell surface and receptor-virus complex internalization via clathrin-mediated endocytosis (17) and viral uncoating triggered by the acidic environment in endosomes or lysosomes. Up to now, SCARB2 is the only receptor known to have three important functions in the EV71 infection cycle, including viral binding, internalization, and uncoating. SCARB2 was demonstrated, by pulldown assays, to bind EV71 virions directly (4). However, as a lysosomal membrane protein, only a tiny amount of SCARB2 is localized on the host cell surface. Hence, EV71 must use multiple alternative attachment receptors to achieve efficient infection.

In contrast to the ubiquitously expressed SCARB2, PSGL-1 (also known as selectin P ligand [SELPLG]) is a type I sialomucin-like membrane protein that is generally expressed in leukocytes, with a role in leukocyte trafficking during inflammation by tethering and rolling leukocytes from blood vessels to activated platelets or endothelia expressing selectins (18). PSGL-1, acting as a receptor for EV71 entry, requires two posttranslational modifications, tyrosine sulfation and glycosylation. Tyrosine sulfation is important for PSGL-1's binding to EV71 via three sulfated tyrosine residues at positions 46, 48, and 51 of the amino terminus (19). Only a subset of specific EV71 strains called PSGL-1-binding strains (PB strains) can use PSGL-1 as an attachment receptor (20). The binding of EV71 to PSGL-1 is mediated by electrostatic interaction (21).

Another vital receptor for EV71, heparan sulfate (HS) is widely distributed on the surface of almost mammalian cell types and in the extracellular matrix as heparan sulfate proteoglycans (HSPGs), which consist of a core protein and unbranched, highly negatively charged

HS polysaccharide side chains. Since HSPGs are hybrid macromolecules consisting of both protein and polysaccharide, their biosynthesis is genetically regulated by two groups of genes encoding the core protein and HS biosynthesis enzymes, respectively. The biosynthesis of HSPG is initiated through the attachment of the first tetrasaccharide to a serine residue of the core protein and then the subsequent addition of the repeating disaccharide units of N-acetylated glucosamine (GlcNAc) and glucuronic acid (GlcA) or iduronic acid (IdoA). The attachment is mediated by five different glycosyltransferases, termed exostosins (EXT1, EXT2, EXTL1, EXTL2, and EXTL3). Next, the *N*-acetyl group of GlcNAc is replaced with a sulfate group, which is catalyzed by four *N*-deacetylase/*N*-sulfotransferases (NDST1, NDST2, NDST3, and NDST4). The subsequent step involves the epimerization of GlcA to IdoA by glucuronyl C5-epimerase (Glce). Finally, *O*-sulfotransferases (OST), including 2-OST, 6-OST, and 3-OST, further modify the HS chains (22). Heparin, mainly found in mast cells, can be viewed as a more sulfated, tissue-specific HS analog. Both HS and heparin are highly negatively charged due to their extensive sulfation modification. Thus, the negative charges of HS or heparin enable them to bind the basic amino acid residues of viral surface proteins with positive charges through electrostatic interactions (23, 24). Due to their ubiquitous expression and structural complexity, HSPGs are hijacked by numerous viruses to attach to target cells. This typically occurs through electrostatic interactions between the negative charges of HSPGs and the basic residues of viral surface glycoproteins of enveloped viruses or viral capsid proteins of nonenveloped viruses. To date, multiple viruses have been reported to exploit these electrostatic interactions to increase their concentration at the cell surface and improve opportunities to bind a more specific entry receptor (25). Some viruses have been proven to be inherent to bind HSPGs, such as dengue virus (DENV) (26), herpes simplex virus (HSV) (27), and human papillomavirus (HPV) (28). Other viruses like foot-and-mouth disease virus (FMDV) (29), coxsackievirus B3 (CV-B3) (30), rhinoviruses C15 (RV-C15) (31), and RV-A8 (32) do not use HSPGs as receptors *in vivo* but become HSPG dependent after adaptation to extensive passages in cultured cells. Interestingly, some viruses, for example, EV71 (33, 34), can even gain HSPG-binding ability *in vivo* after intrahost adaptation. Finally, for other viruses such as respiratory syncytial virus (RSV) (35–37), human parainfluenza virus 3 (HPIV3) (38, 39), and Zika virus (ZIKV) (40–42), their HS dependence remains to be debated because of the controversial data.

The remaining molecules, including VIM, NCL, ANX2, sialylated glycan, DC-SIGN, prohibitin, and fibronectin, were demonstrated to play a role in possible attachment receptors in EV71 infection in *in vitro*-cultured cells (*in vivo* evidence is lacking), as reported in only a single article (43). These molecules can bind and internalize the virus, but they cannot initiate uncoating. They may concentrate EV71 virions on the host cell surface and therefore enhance infectivity by increasing the number of virions that further interact with entry factors. It should be noted that other factors that induce either the uncoating of the captured virions or the thermal degradation of the virions are required to assist these attachment receptors in mediating viral entry and establishing an infection. Therefore, the contributions of these receptors to EV71 infection *in vivo* and the modes of internalization and uncoating remain to be elucidated. Aiming to provide additional evidence for the roles of these possible receptors and to identify host factors, including the remaining novel receptors essential for EV71, a powerful genetic screening tool capable of facilitating a systematic and comprehensive study of EV71 infection is required.

Sulfation, a common modification found in glycoproteins, glycolipids, and proteoglycans (44–46), transfers a sulfate group from the activated form of sulfate 3'-phosphoadenosine-5'-phosphosulfate (PAPS) to a substrate that is catalyzed by various sulfotransferase enzymes. In humans, PAPS is synthesized from two ATPs and one inorganic sulfate ( $\text{SO}_3^-$ ) in the cytoplasm or the nucleus by a two-step process catalyzed by bifunctional PAPS synthases (PAPSS1 and PAPSS2) with both ATP sulfurylase activity and APS kinase activity (47, 48). PAPS serves as the universal sulfate donor for all sulfotransferase enzymes and is mainly transported into the Golgi apparatus by the PAPS transporter for sulfation (49). There are two PAPS transporters, PAPST1 and PAPST2, which are encoded by SLC35B2 and SLC35B3, respectively. After PAPS is delivered into the Golgi apparatus, sulfotransferases are

responsible for the sulfation of specific substrates. Sulfotransferases catalyze the sulfate conjugation of many endogenous and exogenous compounds. According to distinct substrate selectivity and locations for the enzymes, sulfotransferases can be classified into three prominent families: cytosolic sulfotransferases, carbohydrate sulfotransferases, and tyrosyl protein sulfotransferases (TPSTs). Cytosolic sulfotransferases are soluble, and carbohydrate sulfotransferase and TPST are membrane-associated proteins. The other membrane-associated sulfotransferases are all located in the trans-Golgi complex and can be classified into two classes: carbohydrate sulfotransferases and TPSTs. PAPS is thus used in cytoplasmic sulfate transfer reactions, as well as in the lumen of the Golgi apparatus. The carbohydrate sulfotransferases are sulfotransferase enzymes that transfer sulfate to carbohydrate groups in glycolipids, glycoproteins, and proteoglycans (50).

Tyrosine-sulfated proteins are involved in many biological processes, including homeostasis, leukocyte rolling on endothelial cells, viral entry into cells, and ligand binding to receptors (51–53). A series of tyrosine-sulfated proteins have been discovered, whereas only two viral receptors, C-C motif chemokine receptor 5 (CCR5) and PSGL-1, have been reported to undergo protein tyrosine sulfation (PTS). The sulfation of tyrosine residues is essential for the binding and entry of HIV (52), and tyrosine sulfation, but not O-glycosylation, in the N-terminal region of PSGL-1 may facilitate virus entry and the replication of EV71 in leukocytes (19). It is unclear whether well-known EV71 receptors other than PSGL-1 can be sulfated or whether there are unreported host proteins, including novel receptors with tyrosine sulfation, critical for EV71 infection. To address these problems, we need to perform a large-scale genetic screening of EV71.

Genetic screening is an unbiased and comprehensive method used to uncover host cellular components that are critical for infections with viruses. To date, at least two research papers have reported employing genome-wide RNA interference (RNAi)-based knockdown screens to identify host factors that affect EV71 infection. In 2016, Wu et al. conducted a genome-wide immunofluorescence-based RNAi screen in RD cells to identify 256 cellular factors required for EV71 replication (54). In this study, functional validations demonstrated that cyclin-dependent kinase 6 (CDK6) and aurora kinase B (AURKB) act as resistance factors, whereas N-glycanase 1 (NGLY1) is a host susceptibility factor supporting EV71 infection. In 2018, Yeung et al. identified 118 candidate genes and confirmed that human tryptophanyl-tRNA synthetase (hWARS) was important for EV71 entry and infectivity, using genome-wide RNAi library screening in RD cells (55). Despite their widespread use, RNAi screens are reported to have several limitations, such as higher false-positive rates, lower signal-to-noise ratios, more off-target effects, and worse reproducibility than CRISPR-based knockout screens (56, 57). Furthermore, RNAi-based screens reduce gene expression at the transcript level, so they are not successful in completely eliminating gene expression, which leads to a weak or inapparent phenotype, especially when considering the products of target genes with enzymatic activity. In contrast to RNAi-based knockdown screens, the emergence of CRISPR-based knockout screens has ushered in a new era of efficient and large-scale screening efforts, with notable examples including those for *Flaviviridae* family viruses, such as ZIKV, DENV, West Nile virus (WNV), and hepatitis C virus (HCV) (58–61). These studies have successfully identified a series of host dependency genes for virus infection. They have repeatedly illustrated that genome-scale CRISPR screening represents a powerful tool for probing virus-host interactions and identifying new antiviral targets.

We directly obtained the ready-made genome-wide CRISPR-Cas9 knockout (GeCKO) library. After amplifying this library, we produced the pooled lentivirus and then generated a mutant cell pool in HeLa cells. The reason for selecting the HeLa cell line is that it has a broader spectrum of viruses that can infect it, although it is the third most well-known cell line permissive for EV71 infection after RD and Vero. Other kinds of viruses, such as RSV, HPIV3, and ZIKV, can also establish effective infections in HeLa cells. Developing such a HeLa-GeCKO library can serve multiple purposes. We next repeated multiple rounds of the EV71 challenge. The viable cells were finally collected, and deep sequencing was performed. Our screens identified 518 proviral host factors

in the positive selection and 1,044 possible antiviral host factors in the negative selection. We chose the top three candidates in the positive selection, SCARB2, SLC35B2, and B3GAT3, to test whether these genes were essential in EV71 infection and to unravel the mechanism underlying these factors conferring EV71 susceptibility to host cells.

## RESULTS

**CRISPR screening identified host factors essential for EV71 infection.** To identify host factors critical for EV71 infection, we first generated the GeCKO library in EV71-susceptible HeLa cells as previously described (62–64) and performed loss-of-function screening, as illustrated in Fig. 1A. To determine the single guide RNA (sgRNA) distribution of the amplified sgRNA plasmid library, we amplified the sgRNA target region with primers provided by the reference (64) and subjected the purified DNA products to deep sequencing. The quality of the amplified plasmid library was evaluated according to the sgRNA coverage and skew ratio. After analysis of the data, we found that the average sgRNA count was 1,067, the sgRNA coverage was 96.12% (62,848/65,383), and the skew ratio was 8.27 ( $<10$ ). We thus produced a qualified plasmid library and then a stock of sgRNA library lentivirus in HEK293T cells. To avoid introducing multiple sgRNAs into one cell ( $\leq 1$  sgRNA per cell), we employed a low multiplicity of infection (MOI  $< 0.3$ ) with the lentiviral library. Next, the transduced HeLa cells were selected with puromycin to achieve 1,000-fold coverage for each sgRNA in the cell pool. The second round of deep sequencing was performed to evaluate the sgRNA diversity in the HeLa-GeCKO library. The analysis of the obtained 21.9 million reads revealed the presence of 95.83% (62,654/65,383) sgRNAs in the HeLa-GeCKO library, representing an average coverage of  $\sim 260\times$  per sgRNA and a skew ratio of 10.18. The loss of  $\sim 4.9\%$  of the sgRNAs after puromycin selection likely suggests the negative selection of a nonviable cell population. Thus, we successfully generated a pooled GeCKO library in HeLa cells with sufficient coverage to perform genetic screens for EV71-interacting host factors.

To determine the optimal virus level for EV71-induced cell death in HeLa cells for CRISPR screening, we examined EV71-induced cell death following infection at MOIs of 0, 0.01, 0.05, 0.1, 0.5, and 1. As the infection dose of EV71 increased, we gradually observed significant cytopathic effects (CPEs), which included cells that became round and shrunken and eventually detached from the surface of the culture dish into the medium. A nearly 100% CPE was achieved within 48 h postinfection (hpi) at an MOI of  $\geq 0.1$ . For the screen, we chose an MOI of 0.1 to conduct EV71 challenge in HeLa cells. Aiming to strengthen the screening phenotype resistance to EV71, we conducted three rounds of infection at the same MOI of 0.1 and harvested mock-infected cells in parallel. After three rounds of infection, we ensured that there were more than  $3.3 \times 10^7$  surviving cells resistant to EV71. Next, the genomic DNA was extracted from the infected survivor cells and the uninfected populations. It was amplified by PCR and subjected to deep sequencing, followed by bioinformatic analyses. We found that multiple rounds of infection led to a significantly higher skew ratio (data not shown). Based on the sequencing data for these two experimental samples and analysis compared to the control data, we performed a model-based analysis of genome-wide CRISPR-Cas9 knockout (MAGeCK) analysis to identify positively selected genes and obtained two separate gene and sgRNA ranking lists. Then, we performed Pearson correlation analysis to assess the sgRNA representation between two biological replicates, obtaining a good correlation coefficient value of 0.72. For further processing of these results, we combined the two lists according to the average ranking between replicates (gene summary in Table S1 and sgRNA summary in Table S2 in the supplemental material). The screening results are presented as a ranked list of candidates, including 518 hits (called proviral factors) in the positive selection that facilitate EV71 infection and 1,044 hits (some of them called antiviral factors) in the negative selection that may suppress EV71 infection (Fig. 1B). For introducing a selective pressure such as EV71 infection, it is difficult to distinguish between antiviral genes and genes essential for

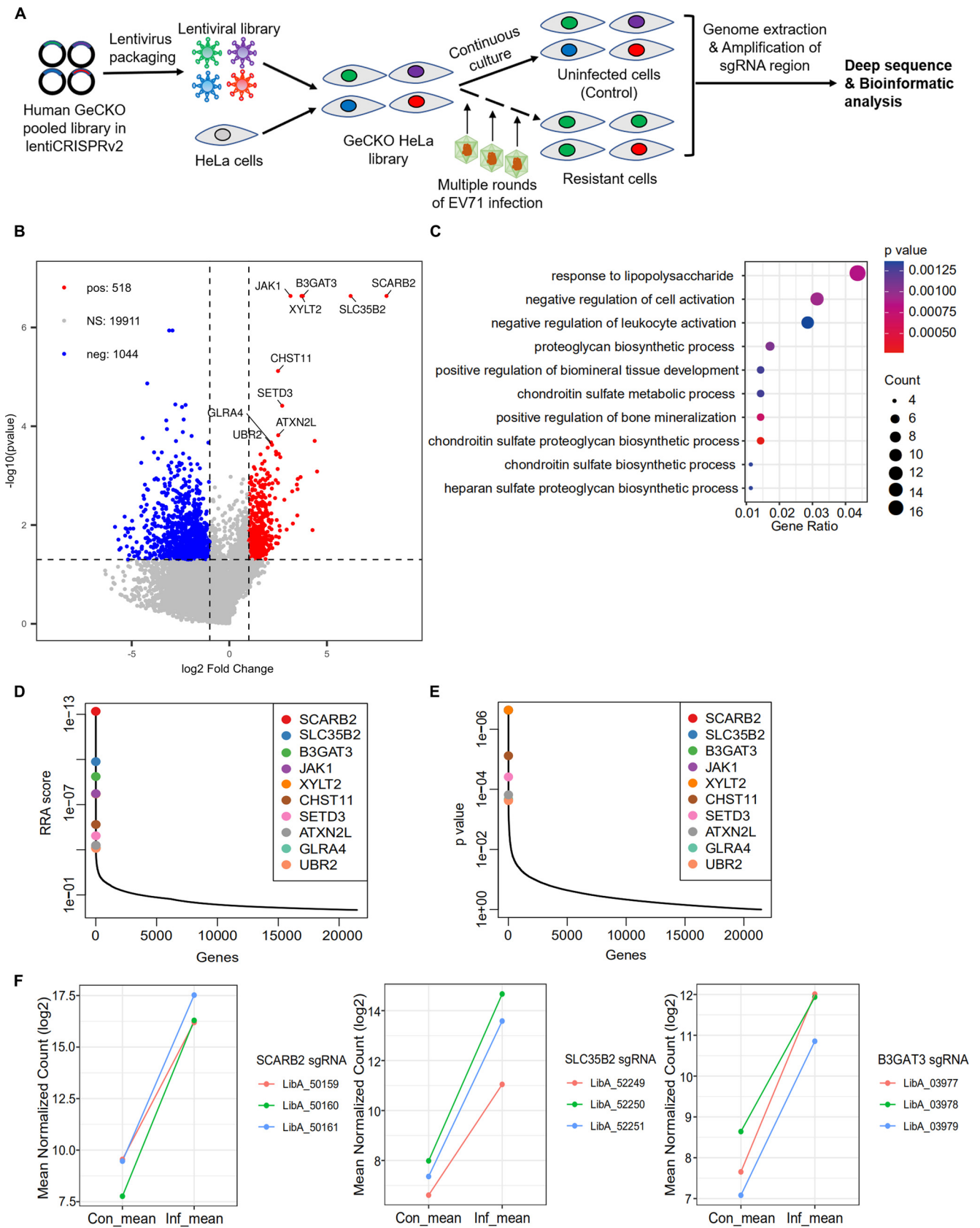


**FIG 1** Genome-wide CRISPR screen for EV71 host dependency factors. (A) Schematic diagram illustrating the workflow of genome-wide CRISPR-Cas9 knockout library screening. Human GeCKO v2 Library-A containing 65,383 sgRNAs was packed into lentiviral particles and transduced into HeLa cells at a (Continued on next page)

host growth and survival. In this study, we focused on the positive selection of the CRISPR screen. The top 10 most enriched candidate genes in the CRISPR-based positive selection screening were SCARB2, SLC35B2, B3GAT3, JAK1, XYLT2, CHST11, SETD3, ATXN2L, GLRA4, and UBR2 (Fig. 1B, D, and E). As expected, the top-hit candidate of this analysis was SCARB2. Moreover, all three sgRNAs independent of SCARB2 were highly enriched, and the values of their logarithmic fold change (LFC) were 8.0514, 8.5235, and 6.6458, respectively (Fig. 1F). Furthermore, SLC35B2, B3GAT3, and XYLT2 are responsible for the synthesis and sulfation modification of HSPGs. This result is supported by a previous report that identified HSPG as an attachment receptor for EV71 infection (9). Collectively, our screening result is convincing. To explore the predicted biological functions of the candidate hits, we performed gene ontology (GO) and Kyoto Encyclopedia of Genes and Genomes (KEGG) pathway enrichment analyses for the top 0.5% ranked genes (~327 genes) from the positive selection. In addition to proteoglycan biosynthesis and modification, these analyses revealed enriched genes involved in response to lipopolysaccharides, negative regulation of cell activation, and positive regulation of biomineral tissue development (Fig. 1C).

Both  $\beta$ -1,3-glucuronyltransferase 3 (B3GAT3) and xylosyltransferase 2 (XYLT2) are enzymes that catalyze the final and first steps, respectively, in forming the tetrasaccharide linkage present in proteoglycans, including heparan sulfate (HS), heparin, chondroitin sulfate (CS), and dermatan sulfate (DS) proteoglycan. In addition to B3GAT3 and XYLT2, another three enzymes (FAM20B, B3GALT6, and B4GALT7), involved in the biosynthesis of the linkage region of proteoglycans, were enriched to a highly significant degree (ranked in the top 64) in the CRISPR-Cas9 screen. All five genes encode the enzymes that catalyze the steps in forming the tetrasaccharide linked to specific serine residues of the core protein. However, no genes except the HS6ST1 gene (ranked 98th, encoding heparan sulfate 6-O-sulfotransferase 1) encoding enzymes that act after the formation of the tetrasaccharide linker, including N-sulfation (NDST1 to -4), C5-epimerization (C5-epimerase), and O-sulfation (HS6ST1 to -3 and HS3ST1, -4, and -5), were identified as enriched. SLC35B2, encoding 3'-phosphoadenosine 5'-phosphosulfate (PAPS) transporter 1 (PAPST1), which mediates the transport of PAPS, a universal sulfuryl donor for sulfation, from the cytosol into the Golgi apparatus, is responsible for host sulfation, including glycosaminoglycan (GAG) sulfation and protein tyrosine sulfation (65). To date, there have been no detailed studies of the relationship between SLC35B2 and EV71. Therefore, we focused on the roles of SLC35B2 in EV71 infection. We then performed a series of validation assays to confirm and characterize the selected EV71 host factors. Notably, the SLC35B2, B3GAT3, and XYLT2 genes were each targeted by three separate sgRNA constructs, all of which were highly enriched, clearly indicating potential EV71 infection-related functions (Fig. 1F). More than 20 genes drive HSPG synthesis and sulfation, and the significant enrichment of specific sgRNAs identified five genes (XYLT2, FAM20B, B3GAT3, B3GALT6, and B4GALT7; top 100 hits) potentially involved in HSPG synthesis and metabolic pathways. Two genes (HS6ST1 and SLC35B2) potentially engaged in sulfation pathways in HeLa cells (66).

#### FIG 1 Legend (Continued)

low multiplicity of infection (MOI < 0.3). The sgRNA-transduced cells were selected using puromycin for 10 days to generate a mutant cell pool. Mutant cells were infected with EV71 at an MOI of 0.1 for 3 rounds. Genomic DNA was extracted from the treated cells, and the sgRNA fragment was amplified by PCR. The copy number of sgRNAs was determined by high-throughput sequencing and analyzed by the MAGECK algorithm. (B) Volcano plot displaying the  $\log_2$  fold change and adjusted  $P$  value for all sgRNAs identified in the screen, revealing that the top three candidates, SCARB2-, SLC35B2-, and B3GAT3-targeting sgRNAs, were positively selected during EV71 infection, suggesting that SCARB2, SLC35B2, and B3GAT3 are genes essential for EV71 to replicate. The horizontal axis (x) indicates the fold change ( $\log_2$ ); the vertical axis (y) denotes the  $P$  value ( $-\log_{10} P$  value). Negative regulators or depleted genes with a  $P$  value threshold of  $\leq 0.05$  are represented by blue dots; positive regulators or enriched genes are represented by red dots. Gray dots represent the genes with no significant differences. (C) KEGG pathway enrichment analysis of the top 1.87% (356/19,050) hits from Inf\_1 and Inf\_2 samples. The vertical axis represents the GO term name, and the horizontal axis represents the corresponding gene ratio of each GO term. The color of the point represents the  $P$  value. The smaller the  $P$  value, the closer the color is to red. The number of differential genes included in each pathway is expressed by the size of the point. The top 10 enriched pathways are represented in the scatterplot. (D and E) The robust rank aggregation (RRA) scores or  $P$  values of top-ranked positively selected genes were calculated using MAGECK. The 10 different-colored dots represent the top 10 essential genes for EV71 replication identified by CRISPR screenings. A minor RRA score determined by the MAGECK algorithm indicates a more robust selection of the corresponding gene. The results were based on two biologically independent screens. (F)  $\log_2$ -transformed mean normalized read counts for sgRNAs targeting SCARB2 (left), SLC35B2 (middle), and B3GAT3 (right) in control (uninfected) and infected samples.

**Knockout of SCARB2, SLC35B2, or B3GAT3 significantly inhibits EV71 infection.**

To investigate whether SCARB2, SLC35B2, or B3GAT3 was critical for EV71 replication, we first generated individual knockout (KO) cells of SCARB2, SLC35B2, and B3GAT3 in the HeLa cell line using the CRISPR-Cas9 editing system. The clonal KO cell lines were confirmed with endogenous antibodies, anti-SCARB2 and anti-B3GAT3 antibodies (Fig. 2A). In addition, the sequencing of the predicted target sites confirmed that each of these KO cell lines had one or more nucleotide indels expected to cause a frameshift mutation in the coding regions of the targeted gene (a noninteger multiple of three) (Fig. 2I). Due to the lack of a working anti-SLC35B2 antibody, there is no corresponding Western blot assay for the SLC35B2 KO clone. Moreover, the results of the cell proliferation ability assays showed no difference in cell proliferation rates between corresponding KO and HeLa wild-type (WT) cells (Fig. 2D). To determine the stage at which the genes disrupted in our clones conferred resistance to EV71 infection, we analyzed the time course of replication by quantitative real-time PCR (RT-qPCR) in different cell clones (Fig. 2B). The results showed a remarkable increase in viral RNA production as early as 6 h after the EV71 challenge in HeLa WT cells. However, this was dramatically reduced in the SCARB2<sup>KO</sup>, SLC35B2<sup>KO</sup>, and B3GAT3<sup>KO</sup> cells. Expressly, at 12 hpi, the loss of SCARB2 conferred the most robust resistance against EV71 infection, which showed an ~1,000-fold reduction in the EV71 mRNA level. In contrast, the mRNA level of EV71-encoded P1 polyprotein in SLC35B2<sup>KO</sup> and B3GAT3<sup>KO</sup> cells was modestly reduced (~125-fold) or minimally reduced (~30-fold). In addition, at 2 hpi, we observed that the viral mRNA level of SCARB2<sup>KO</sup> cells was nearly equal to that of WT cells. In comparison, the SLC35B2<sup>KO</sup> and B3GAT3<sup>KO</sup> clones showed more than 60% reduction in the viral mRNA level at 2 hpi. Accordingly, the resistance mechanism for the SLC35B2 and B3GAT3 KO clones most likely involves the attachment or entry phase. In agreement with the reduced viral mRNA level observed in the KO clones, the results from immunoblotting analyses showed that the expression of the EV71-encoded VP1 protein in all three KO clones (SCARB2<sup>KO</sup>, SLC35B2<sup>KO</sup>, and B3GAT3<sup>KO</sup>) was dramatically reduced or even undetectable following EV71 infection, exhibiting robust resistance against EV71 infection (Fig. 2C, compare lanes 6, 7, and 8 to lane 5; compare lanes 10, 11, and 12 to lane 9).

To confirm the above findings, we also generated SCARB2, SLC35B2, and B3GAT3 KO clones using the human RD cell line (Fig. 2E and J) and repeated the time course of infection experiments. CCK-8 assays showed no difference in cell viability between KO and WT cells (Fig. 2H). As described above for HeLa cells, the knockout of SCARB2, SLC35B2, and B3GAT3 in RD cells resulted in obvious inhibition of EV71 infection (Fig. 2F and G).

To determine whether the role of these genes was specific to the test virus, we next infected HeLa WT cells and the corresponding KO cells with other RNA viruses available in our laboratory. For this purpose, we additionally infected HeLa WT cells and SCARB2<sup>KO</sup>, SLC35B2<sup>KO</sup>, and B3GAT3<sup>KO</sup> cells with RSV, HPIV3, and ZIKV (Fig. 2K to M). A comparable dependency on the SLC35B2 and B3GAT3 genes, not SCARB2, was also observed for RSV (Fig. 2K). For HPIV3, the knockout of SCARB2, SLC35B2, or B3GAT3 did not affect the viral protein HN level (Fig. 2L). The results revealed that SCARB2, SLC35B2, or B3GAT3 is not necessary for HPIV3 replication. For ZIKV, the knockout of SCARB2 or SLC35B2 slightly inhibited ZIKV infection. Interestingly, however, the knockout of B3GAT3 significantly promoted ZIKV replication (Fig. 2M). These results indicated that SLC35B2 might be a panproviral host factor.

**Reconstitution of SCARB2, SLC35B2, or B3GAT3 restores the infectivity of EV71.**

To exclude the possible off-target effects in the KO clones, we performed rescue experiments. We constructed a series of stably transfected cells using a lentiviral expression vector, pCDH-CMV-IRES-MCS-SF-BLAST, equipped with a C-terminal Flag tag. The KO clones were reintroduced with the empty vector, designated SCARB2<sup>VEC</sup>, SLC35B2<sup>VEC</sup>, and B3GAT3<sup>VEC</sup>. The KO clones were complemented with full-length cDNA encoding the WT products, and these cell lines were designated SCARB2<sup>RES</sup>, SLC35B2<sup>RES</sup>, and B3GAT3<sup>RES</sup>, respectively. In addition, SLC35B2<sup>KO</sup> and B3GAT3<sup>KO</sup> clones were transduced with an enzymatically inactive mutant, designated SLC35B2<sup>G127E</sup> and B3GAT3<sup>D194A&D195A</sup> (or B3GAT3<sup>2DA</sup>), respectively (67). The retroviral expression of C-terminally Flag-tagged SCARB2, SLC35B2,



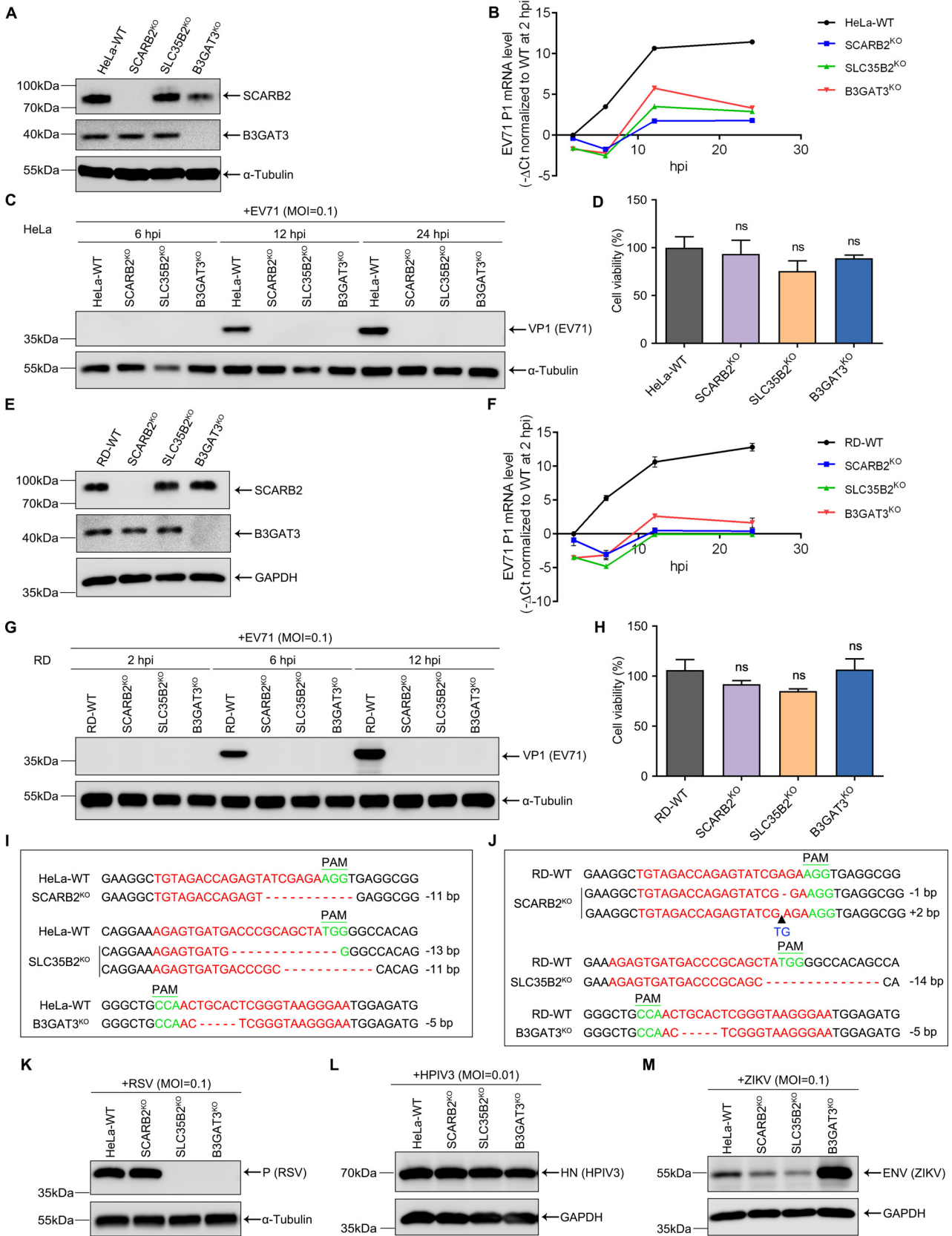


**FIG 2** Knockout of SCARB2, SLC35B2, or B3GAT3 confers strong protection against EV71 infection. (A and E) Western blot analyses of SCARB2 and B3GAT3 proteins in HeLa or RD wild-type (WT) cells and the corresponding SCARB2<sup>KO</sup>, SLC35B2<sup>KO</sup>, and B3GAT3<sup>KO</sup> cell clones. Endogenous  $\alpha$ -tubulin (Continued on next page)

and B3GAT3 fully restored the susceptibility to EV71 infection, with a level of VP1 comparable to that of the WT cells. In contrast, both enzymatically inactive mutants SLC35B2<sup>G127E</sup> and B3GAT3<sup>D194A&D195A</sup> failed to restore the susceptibility to EV71 infection (Fig. 3A to F). Our data suggest that in both HeLa and RD cells, SCARB2, SLC35B2, and B3GAT3 are required for efficient EV71 infection.

**SLC35B2 and B3GAT3, not SCARB2, are required for EV71 attachment and internalization.** Having confirmed the importance of SCARB2, SLC35B2, and B3GAT3 in facilitating EV71 infection, we next determined which stage of the viral life cycle was affected in the KO clones. To this end, we performed virus binding and internalization assays with an RT-qPCR-based method to quantify the EV71 virions bound to the cells or internalized into cells (68). For the binding assay, we incubated WT, SCARB2<sup>KO</sup>, SLC35B2<sup>KO</sup>, and B3GAT3<sup>KO</sup> cells with EV71 for 1 h at 4°C. EV71 virions bound to the cells were subjected to RT-qPCR analysis. As shown in Fig. 4A and B, in both HeLa and RD cell lines, a similar significant reduction in the binding of EV71 particles was observed in SLC35B2<sup>KO</sup> and B3GAT3<sup>KO</sup> cells, compared to WT cells. However, there was no significant difference in the binding of the virions between SCARB2<sup>KO</sup> and WT cells. For the internalization assay, we incubated WT, SCARB2<sup>KO</sup>, SLC35B2<sup>KO</sup>, and B3GAT3<sup>KO</sup> cells with EV71 for another 1 h at 37°C, closely following the EV71 binding assay. The results show that the reduction in internalized EV71 virions was more remarkable among SLC35B2<sup>KO</sup> and B3GAT3<sup>KO</sup> cells than WT cells, whereas the knockout of SCARB2 did not affect EV71 attachment or internalization (Fig. 4D and E). Next, to confirm that EV71 bound to SCARB2<sup>KO</sup> cells more efficiently than to SLC35B2<sup>KO</sup> and B3GAT3<sup>KO</sup> cells, we performed an immunofluorescence analysis to compare the numbers of cell surface-attached and intracellular internalized EV71 virions. We used 1,1'-dioctadecyl-3,3',3'-tetramethylindocarbocyanine perchlorate (Dil), a fluorescent compound, in this study. As shown in Fig. 4C, Dil-labeled virions were added to cultured cells and incubated for 1 h at 4°C, and fewer viral particles were attached to SLC35B2<sup>KO</sup> and B3GAT3<sup>KO</sup> cells than to WT cells. SLC35B2<sup>KO</sup> and B3GAT3<sup>KO</sup> cells showed reduced binding levels of 98.5% and 99.1%, respectively, compared to 100% for WT cells. The internalization of Dil-labeled EV71 virions into cells was performed as described in Materials and Methods. As shown in Fig. 4F, significantly fewer Dil-labeled virions were internalized into SLC35B2<sup>KO</sup> and B3GAT3<sup>KO</sup> cells than into WT cells. SLC35B2<sup>KO</sup> and B3GAT3<sup>KO</sup> cells showed reduced internalization levels of 99.1% and 98.7%, respectively, compared to the 100% for WT cells. However, the knockout of SCARB2 did not affect EV71 binding (a reduced binding level of 4.1%) or internalization (a reduced internalization level of 3.9%) because of similar levels of Dil-labeled EV71 virions observed in both SCARB2<sup>KO</sup> and WT cells. In addition, to compare the efficiencies of EV71 binding in HeLa cell lines that were deficient in SCARB2, SLC35B2, or B3GAT3, we conducted flow cytometry analysis based on Dil-labeled virions to confirm the previous binding assays. According to the flow cytometric analysis, the number of Dil-positive wild-type cells and

## FIG 2 Legend (Continued)

was used as a loading control. There is no applicable antibody available for SLC35B2; its knockout clone was confirmed by Sanger sequencing. (B and F) A time course infection experiment monitoring the relative mRNA level of EV71 P1 gene in HeLa or RD WT cells and corresponding SCARB2<sup>KO</sup>, SLC35B2<sup>KO</sup>, and B3GAT3<sup>KO</sup> cell clones was conducted using RT-qPCR analysis. After EV71 challenge, cells were harvested at the indicated hours postinfection (2, 6, 12, and 24 hpi) for RT-qPCR analysis. The glyceraldehyde 3-phosphate dehydrogenase (GAPDH) housekeeping gene was used as an internal control. Error bars, mean  $\pm$  standard deviation (SD) of the results of three independent experiments. (C and G) A time course infection experiment detecting EV71 VP1 protein expression in HeLa or RD WT cells and corresponding SCARB2<sup>KO</sup>, SLC35B2<sup>KO</sup>, and B3GAT3<sup>KO</sup> cell clones was performed by Western blot analysis. After EV71 challenge, cells were harvested at the indicated hours postinfection for Western blot analysis. Endogenous  $\alpha$ -tubulin was used as a loading control. (D and H) CCK-8 cytotoxicity assay in HeLa cells and RD cells. Cells were seeded into a 96-well plate and incubated with different concentrations of sodium chlorate for 24 h, followed by the addition of 10  $\mu$ L of the CCK-8 solution to each well and incubation for 2 h in the incubator (at 37°C and 5% CO<sub>2</sub>). The absorbance at 450 nm was measured using a microplate reader. Experiments were repeated three times, and results are presented as the mean  $\pm$  SD. (I and J) Alignment of the nucleic acid sequences of three clonal HeLa KO cells or RD KO cells of SCARB2, SLC35B2, and B3GAT3 with WT cells and by Sanger sequencing. The sgRNA targeting sites are highlighted in red. The red dashes indicate the deleted bases, the black triangle indicates the inserted site in the KO clone, and the inserted bases are shown in blue letters below the sequence. The protospacer adjacent motif (PAM) site is indicated in green lettering. (K to M) Western blotting was performed to examine the expression levels of the P protein, HN protein, and ENV protein in SCARB2<sup>KO</sup>, SLC35B2<sup>KO</sup>, and B3GAT3<sup>KO</sup> clones following infection with RSV at an MOI of 0.1 (K), HPIV3 at an MOI of 0.01 (L), and ZIKV at an MOI of 0.1 (M), respectively. Endogenous  $\alpha$ -tubulin or GAPDH was used as an internal control.

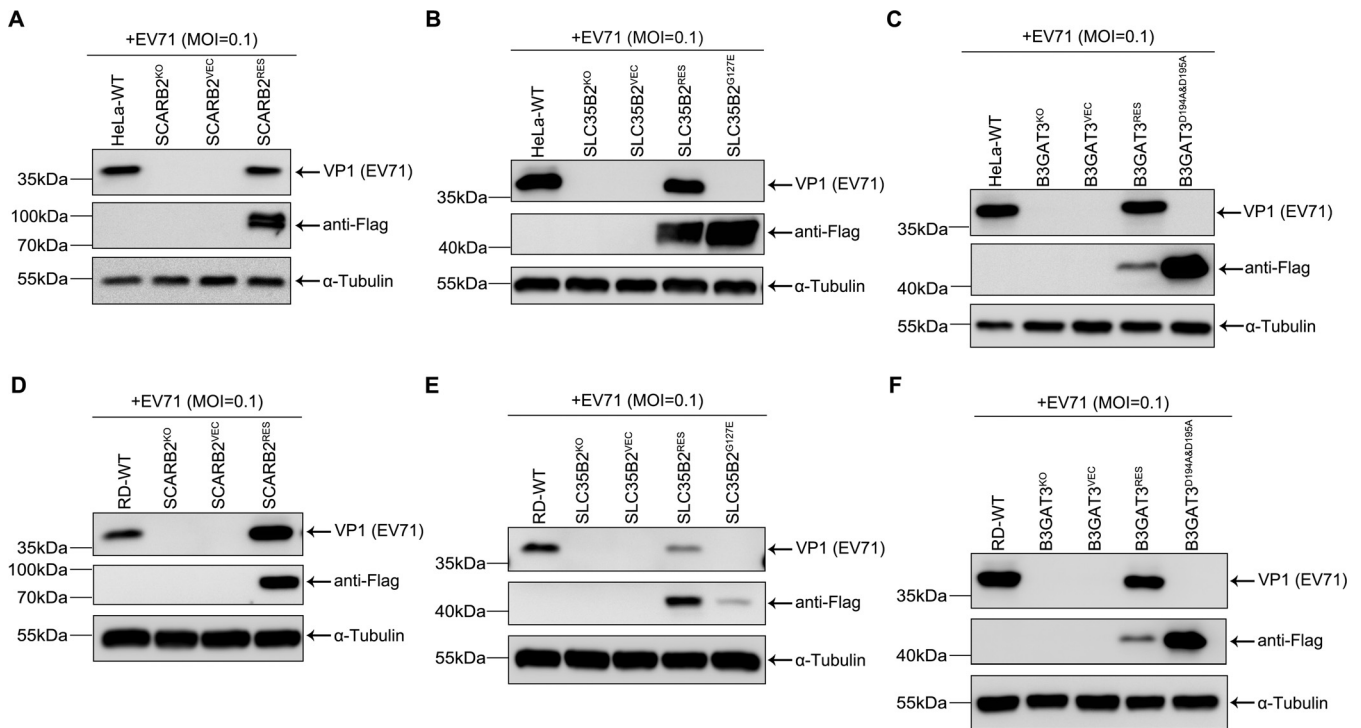


**FIG 3** Reconstitution of SCARB2, SLC35B2, or B3GAT3 restores the infectivity of EV71. (A and D) Rescue assays for retroviral expression of SCARB2 in SCARB2<sup>KO</sup> cells. We developed two cell lines that were stably transfected with empty lentiviral vector pCDH-MCS (i.e., SCARB2<sup>VEC</sup>) and a C-terminally Flag-tagged SCARB2 full-length transcript with synonymous mutations in the target region (i.e., SCARB2<sup>RES</sup>), respectively. Western blotting was performed to determine the VP1 level of HeLa cells (A) and RD cells (D) after EV71 infection. Endogenous  $\alpha$ -tubulin was used as a loading control. (B and E) Rescue assays for retroviral expression of SLC35B2 in SLC35B2<sup>KO</sup> cells. We developed three cell lines that were stably transfected with empty lentiviral vector pCDH-MCS (i.e., SLC35B2<sup>VEC</sup>), a C-terminally Flag-tagged SLC35B2 full-length transcript with synonymous mutations in the target region (i.e., SLC35B2<sup>RES</sup>), and a SLC35B2 enzymatically inactive mutant at site 127 (i.e., SLC35B2<sup>G127E</sup>), respectively. Western blotting was performed to determine the VP1 level of HeLa cells (B) and RD cells (E) after EV71 infection. Endogenous  $\alpha$ -tubulin was used as a loading control. (C and F) Rescue assays for retroviral expression of B3GAT3 in B3GAT3<sup>KO</sup> cells. We developed three cell lines that were stably transfected with empty lentiviral vector pCDH-MCS (i.e., B3GAT3<sup>VEC</sup>), a C-terminally Flag-tagged B3GAT3 full-length transcript with synonymous mutations in the target region (i.e., B3GAT3<sup>RES</sup>), and a B3GAT3 enzymatically inactive mutant at two sites, 194 and 195 (i.e., B3GAT3<sup>D194A&D195A</sup> or B3GAT3<sup>2DA</sup>), respectively. Western blotting was performed to determine the VP1 level of HeLa cells (C) and RD cells (F) after EV71 infection. Endogenous  $\alpha$ -tubulin was used as a loading control.

SCARB2<sup>KO</sup> cells was significantly greater than that of the SLC35B2<sup>KO</sup> and B3GAT3<sup>KO</sup> cells (Fig. 4G) ( $P = 0.9124, 0.0114, \text{ and } 0.01332$ , respectively). These results led to the same conclusion that SLC35B2 and B3GAT3 are essential for EV71 attachment but SCARB2 is not. Our result is consistent with a published report showing that pretreating cells with a SCARB2 antibody had less influence on virus binding than pretreating cells with a vimentin antibody or PSGL-1 antibody (8). One possible explanation is that in the presence of multiple attachment receptors, especially HS, which is abundantly expressed in many cell lines, including HeLa and RD cell lines, the contribution of SCARB2, which is rarely distributed on the cell surface, to viral binding and internalization can be negligible.

To exclude the possibility of other phases in the viral life cycle, we performed another RT-qPCR assay to determine the relative viral RNA level after the transfection of the EV71 genome RNA transcribed *in vitro*. As shown in Fig. 4H and I, regardless of the HeLa or RD cell line, there was no statistically significant difference in the EV71 RNA levels between the SLC35B2 and B3GAT3 KO clones and WT cells at 12 h post-transfection (hpt). Considering the time course of EV71 replication described above, although we observed a lower viral RNA level in SLC35B2<sup>KO</sup> or B3GAT3<sup>KO</sup> cells than in SCARB2<sup>KO</sup> cells at 2 and 6 hpi, the knockout of SCARB2 in both the HeLa and RD cell lines resulted in the most significant degree of resistance to EV71 infection at 12 hpi (Fig. 2B and F). In addition, compared with WT cells, SCARB2<sup>KO</sup> cells exhibited a significant inhibition in EV71 replication as early as 6 hpi. We could infer from these data that the knockout of SCARB2 affects EV71 infection at 2 to 6 hpi (after internalization but

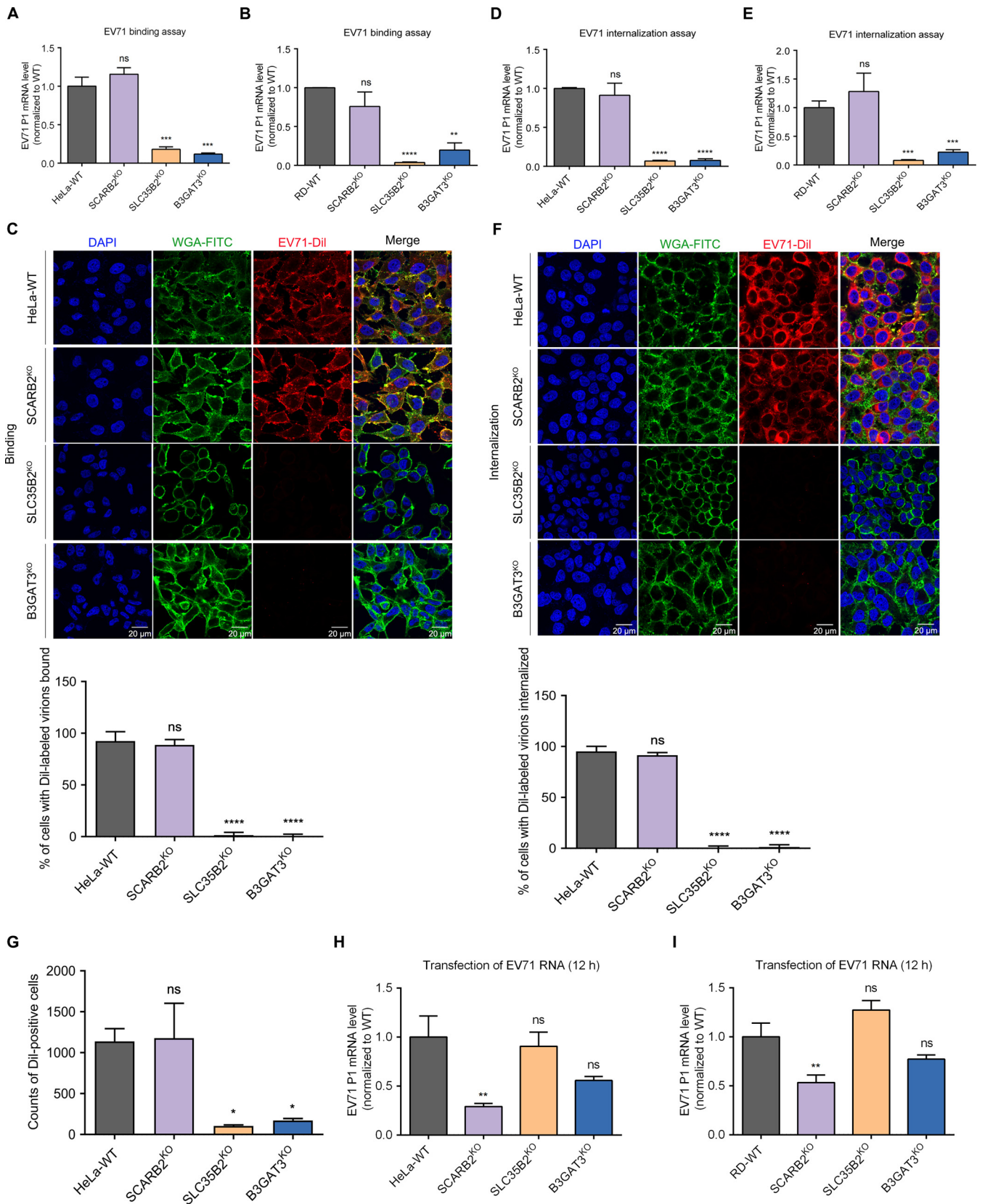


**FIG 4** SLC35B2 and B3GAT3, not SCARB2, are required for EV71 attachment and internalization. (A and B) Analysis of the binding of EV71 to HeLa or RD WT cells and the corresponding KO cells using RT-qPCR. Cells were incubated with the virus at an MOI of 5 for 1 h at 4°C. After several washes to remove unbound viral particles, RNA was extracted for RT-qPCR analysis. EV71 RNA copy numbers were normalized to the mean values for WT cells in each assay. (Continued on next page)

before genome RNA replication). This time frame exactly corresponds to the uncoating step of the EV71 replication cycle. Thus, in both HeLa and RD cell lines, SCARB2 probably plays a vital role in the viral uncoating step and a relatively minor role in the attachment and internalization in viral entry.

**Host sulfation is critical for EV71 entry.** To determine if SLC35B2 could act as a vital modulator for host sulfation, we first evaluated the sulfation levels of different KO clones by radioactive isotope labeling. We labeled the individual KO and WT cells with  $^{35}\text{SO}_4^{2-}$  for 36 h and then observed the sulfation profile by autoradiography. The autoradiogram control showed identical incorporation of  $^{35}\text{S}$ Met/ $^{35}\text{S}$ Cys in the KO clones and WT cells (Fig. 5A, left panel). Under the circumstances, the sulfation profile of the SCARB2<sup>KO</sup> cells was the same as that of the WT cells (Fig. 5A, right panel, lanes 1 and 3). However, the B3GAT3<sup>KO</sup> clone displayed an ~100% reduction in the incorporation of  $^{35}\text{SO}_4^{2-}$  into high-molecular-weight (high-MW) molecules (>170 kDa, near the top of the gel) compared to the WT cells, with the nearly complete loss of sulfated proteoglycans (Fig. 5A, right panel, lanes 1 and 4). In comparison, the SLC35B2<sup>KO</sup> clone showed a reduction of ~95%, retaining a portion of sulfated high-MW molecules (Fig. 5A, right panel, lanes 1 and 2). Notably, on the autoradiograph of  $^{35}\text{SO}_4$ -labeled cell-associated materials resolved by SDS-PAGE, dark smears near the top of the gel at >170 kDa were reported to be HSPGs, consisting of a core protein and one or more covalently attached glycosaminoglycans (GAGs) (67). There was no smear in the WT and KO clones labeled with  $^{35}\text{S}$ Met/ $^{35}\text{S}$ Cys, because only proteins, and not GAGs, could be labeled by  $^{35}\text{S}$ Met/ $^{35}\text{S}$ Cys (Fig. 5B, left panel). Thus, the bands at >170 kDa probably referred to core proteins of HSPG on the autoradiograph of  $^{35}\text{S}$ Met/ $^{35}\text{S}$ Cys-labeled cell-associated materials (Fig. 5A, left panel). The B3GAT3<sup>KO</sup> cells were completely unable to produce HSPGs, but there remained quite a few sulfated proteins (<170 kDa) (Fig. 5A, right panel, lane 4). However, no apparent bands at <170 kDa could be detected in the SLC35B2<sup>KO</sup> clone (Fig. 5A, right panel, lane 2), which indicated that SLC35B2 knockout resulted in blocking of the sulfation pathway responsible for the whole cellular proteins. The inability of the B3GAT3<sup>KO</sup> clone or SLC35B2<sup>KO</sup> clone to produce heparan sulfate and the ability of the SCARB2<sup>KO</sup> clone to still yield heparan sulfate at ~100% of WT levels were seen in the KO clones by immunofluorescence assays with an antibody against heparan sulfate/heparin (10E4; data not shown).

To exclude the potential off-target effects, we performed rescue experiments to

#### FIG 4 Legend (Continued)

Data are presented as means  $\pm$  SD;  $n = 3$ .  $P$  values were generated using an unpaired two-tailed Student  $t$  test. ns, not significant at  $P > 0.05$ ; \*,  $P < 0.05$ ; \*\*,  $P < 0.01$ ; \*\*\*,  $P < 0.001$ ; \*\*\*\*,  $P < 0.0001$ . (C) Analysis of the binding of Dil-labeled EV71 virions to HeLa WT cells and the corresponding KO cells using immunofluorescence. Cells were cultured on glass coverslips overnight. Dil-labeled virions were added to cultured cells and incubated for 1 h at 4°C. The unbound virus was washed off with cold PBS three times. The cells were fixed with 4% paraformaldehyde for 20 min at room temperature. Cell nuclei were stained with DAPI, and cell membranes were stained with WGA-FITC. Then, the cells were observed under a Leica confocal microscope fitted with a 100 $\times$  objective lens. The red particles are Dil-labeled EV71 virions. The green-colored rings are cell membranes. The blue dots are cell nuclei. DAPI, 4',6-diamidino-2-phenylindole; WGA-FITC, wheat germ agglutinin-fluorescein isothiocyanate conjugate. Scale bar, 20  $\mu\text{m}$ . The accompanying bar graph represents the percentages of cells attached with Dil-labeled EV71 virions. (D and E) Analysis of the amount of EV71 virions internalized into HeLa or RD WT cells and the corresponding KO cells using RT-qPCR. Cells were incubated with EV71 at an MOI of 5 for 1 h at 4°C and then washed 3 times with ice-cold PBS. After addition of fresh complete DMEM, cells were incubated at 37°C for another 1 h to allow virus internalization. Next, the cells were treated with 1 mL of trypsin to detach them from the plate and remove surface-bound virions that did not internalize. After three washes, the total RNA of the cells was extracted for RT-qPCR analysis. EV71 RNA copy numbers were normalized to the mean values for WT cells in each assay. (F) Analysis of the amount of EV71 virions internalized into RD WT cells and the corresponding KO cells using immunofluorescence. Cells were incubated with the virus at an MOI of 5 for 1 h at 4°C and then gently washed 3 times with ice-cold PBS. After addition of fresh complete DMEM, cells were incubated at 37°C for another 1 h to allow virus internalization. The cells were fixed with 4% paraformaldehyde for 20 min. Cell nuclei were stained with DAPI, cell membrane was stained with WGA-FITC, and then the cells were observed under a Leica confocal microscope fitted with a 100 $\times$  objective lens. The red particles are Dil-labeled EV71 virions. The green-colored rings are cell membranes. The blue dots are cell nuclei. Scale bar, 20  $\mu\text{m}$ . The accompanying bar graph represents the percentages of cells with internalized Dil-labeled EV71 virions. (G) Dil-labeled EV71 virions on the cell surface, as measured by flow cytometry. Cells were trypsinized and harvested by centrifugation at 4,000 rpm for 2 min at 4°C. As a negative control, HeLa cells were stained with Dil-labeled medium instead of Dil-labeled virus. Dil-labeled virions were added to trypsinized cells and incubated for 1 h at 4°C. The unbound virus was washed off with ice-cold PBS three times. Then, cells were resuspended in ice-cold PBS, 3% BSA, and 1% sodium azide and then analyzed on the flow cytometer. The number of cells bound to Dil-labeled EV71 is determined by flow cytometry (10<sup>4</sup> cells per experiment). The flow cytometry data are shown as the mean count  $\pm$  SD. ns, not significant at  $P > 0.05$ ; \*,  $P < 0.05$ ; \*\*,  $P < 0.01$ ; \*\*\*,  $P < 0.001$ ; \*\*\*\*,  $P < 0.0001$  according to Student's  $t$  test. (H and I) RT-qPCR assay for determination of relative mRNA level for the EV71 P1 gene after transfection of the EV71 genome RNA transcribed *in vitro* into HeLa or RD WT, SCARB2<sup>KO</sup>, SLC35B2<sup>KO</sup>, and B3GAT3<sup>KO</sup> cells. At 12 hpt, total RNA was extracted for RT-qPCR analysis. Endogenous GAPDH served as the internal reference.

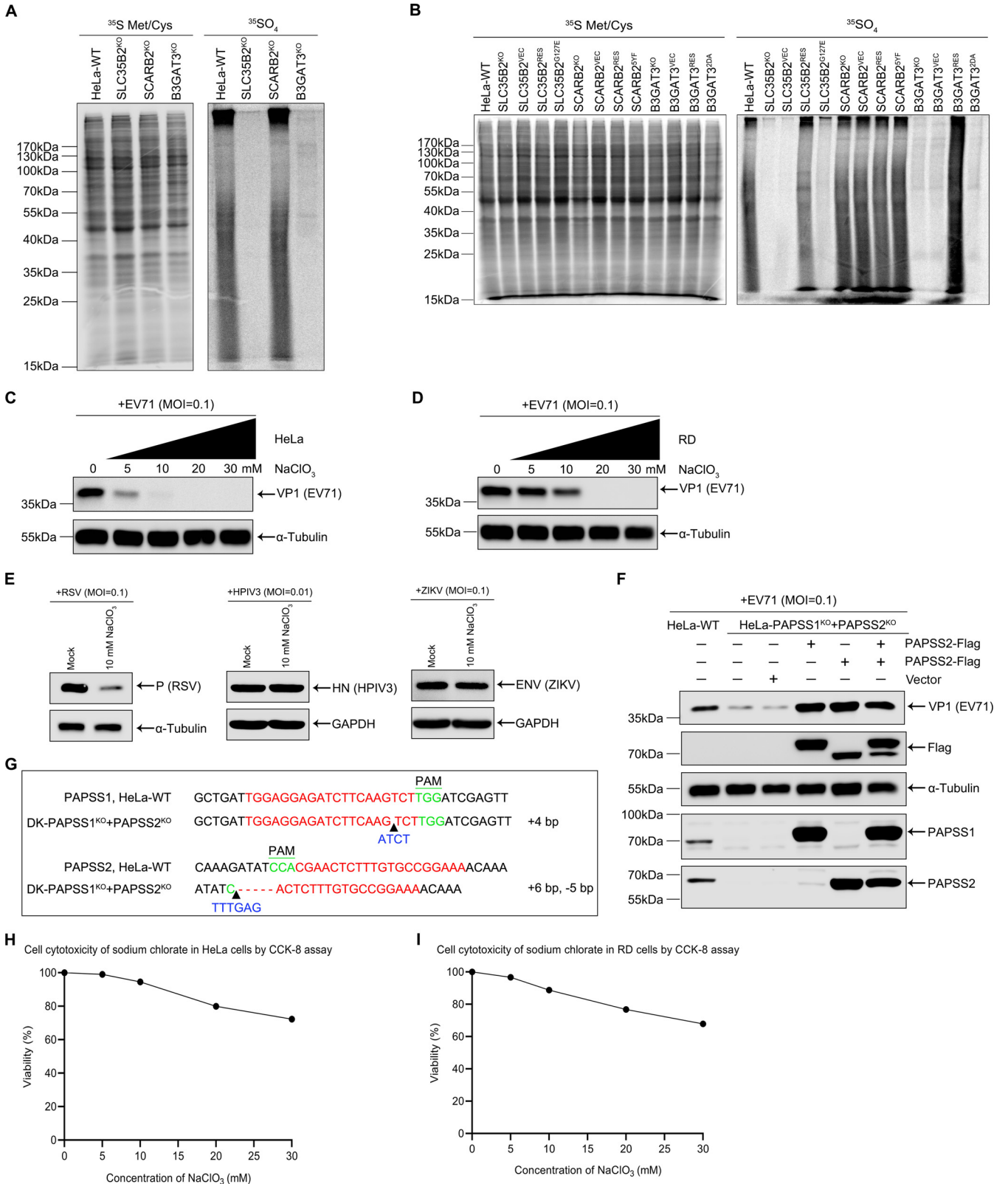


**FIG 5** Sulfation is critical for EV71 entry. (A and B) Metabolic labeling with sulfate to evaluate cellular sulfation level in different KO clones, the reconstituted clones with the empty expression vector, the reconstituted clones with respective WT transcripts, and the reconstituted clones with enzymatically inactive mutants or specific mutants. Cells were seeded into six-well plates until they achieved ~70% confluence, 100  $\mu$ Ci/mL [<sup>35</sup>S]<sub>4</sub> or 33  $\mu$ Ci/mL [<sup>35</sup>S]methionine/[<sup>35</sup>S]cysteine was added to the medium in each plate, and the cells were left to reach steady state for ~36 h. Labeled cells were harvested and lysed in lysis buffer on ice. Then, the lysates were resolved on an SDS-PAGE gel; the gel was dried and then exposed to a phosphorimager (Continued on next page)

demonstrate complementation by the empty vector, the full-length genes, and their enzymatically inactive mutants. As shown in Fig. 5B, there was a significant reduction in incorporation of  $^{35}\text{SO}_4$  in the B3GAT3<sup>KO</sup>, B3GAT3<sup>VEC</sup>, and B3GAT3<sup>2DA</sup> clones (Fig. 5B, right panel, lanes 10, 11, and 13, respectively) compared with the reconstituted B3GAT3<sup>RES</sup> and WT clone (Fig. 5B, right panel, lanes 12 and 1, respectively). As for SLC35B2, there was no incorporation of  $^{35}\text{SO}_4$  in the SLC35B2<sup>KO</sup>, SLC35B2<sup>VEC</sup>, or SLC35B2<sup>G127E</sup> clone (Fig. 5B, right panel, lanes 2, 3, and 5, respectively) compared with the reconstituted SLC35B2<sup>RES</sup> and WT clone (Fig. 5B, right panel, lanes 4 and 1, respectively). Expectedly, there was no significant difference in the sulfation levels among these groups of SCARB2<sup>KO</sup>, SCARB2<sup>VEC</sup>, SCARB2<sup>RES</sup>, and SCARB2<sup>5YF</sup> clones (the SCARB2<sup>KO</sup> clone with retroviral expression of the SCARB2 mutant which had five tyrosine-to-phenylalanine substitutions, including Y7F, Y198F, Y267F, Y284F, and Y410F, was termed SCARB2<sup>5YF</sup>) and WT clones (Fig. 5B, right panel, lanes 6, 7, 8, 9, and 1, respectively).

The  $^{35}\text{SO}_4$ -labeled SLC35B2<sup>RES</sup>, B3GAT3<sup>RES</sup>, and WT clones showed a mass of smears at >170 kDa, whereas the number of smears of the  $^{35}\text{SO}_4$ -labeled SLC35B2<sup>KO</sup>, SLC35B2<sup>VEC</sup>, and SLC35B2<sup>G127E</sup> clones remained low (~5%). In comparison, the  $^{35}\text{SO}_4$ -labeled B3GAT3<sup>KO</sup>, B3GAT3<sup>VEC</sup>, and B3GAT3<sup>2DA</sup> clones had no smear in the same position (Fig. 5B, right panel, lanes 10, 11, and 13, respectively). This means that B3GAT3-deficient cells cannot produce any heparan sulfate, whereas SLC35B2-deficient cells still yield heparan sulfate at ~5% of the WT levels. Moreover, the B3GAT3<sup>KO</sup> clone produced more sulfated proteins at <170 kDa than the SLC35B2<sup>KO</sup> clone. However, the knockout of SLC35B2 imparted greater resistance to EV71 than the knockout of B3GAT3 at 12 hpi (Fig. 2B), suggesting that besides HSPGs, some sulfated proteins are critical for EV71 infection (Fig. 5B, right panel, lane 2). In other words, SLC35B2 indirectly affected EV71 infection by mediating two types of sulfation, including GAG sulfation and protein tyrosine sulfation. We could speculate that all the sulfated proteins present in the SLC35B2<sup>RES</sup> clone and absent from the SLC35B2<sup>KO</sup> clone are candidates for proteins involved in EV71 replication.

To further confirm the role of host sulfation in EV71 attachment and entry, we performed EV71 infection of HeLa cells grown in a medium containing 0 to 30 mM sodium chlorate. As shown in Fig. 5C, HeLa cells pretreated with various concentrations of sodium chlorate showed a concentration-dependent reduction in expression of the VP1 protein following EV71 infection. Even with a concentration as low as 10 mM, the percentage of viral RNA inhibition was >90%, and significant inhibition of capsid protein synthesis was observed. To rule out the possibility that the reduction in the level of EV71 infection was due to cytotoxicity, we conducted a cytotoxicity test for sodium chlorate using a cell counting kit-8 (CCK-8). The data revealed that sodium chlorate had minimal cytotoxicity at 10 mM (viability of >90% compared to untreated cells) (Fig. 5H). We then chose 10 mM sodium chlorate to test the other three RNA viruses. At 10 mM, sodium chlorate significantly inhibited the replication of RSV as well as EV71, while HPIV3 and ZIKV were not affected by sodium chlorate at the same concentration (Fig. 5E). These results are consistent with the immunoblotting analysis in the SLC35B2<sup>KO</sup> clone, supporting the idea that sodium chlorate inhibits EV71 replication by abolishing host sulfation. Then, we conducted EV71 infection

#### FIG 5 Legend (Continued)

screen. (C and D) Inhibitory effect of sodium chlorate on EV71 in HeLa or RD cells. Cells were pretreated with increasing concentrations (0 to 30 mM) of sodium chlorate for 24 h before EV71 infection at an MOI of 0.1. The cells were harvested for whole-cell extract preparation and Western blotting to detect EV71 VP1 protein.  $\alpha$ -Tubulin was used as an internal control. (E) Inhibitory effect of sodium chlorate on RSV (left), HPIV3 (middle), and ZIKV (right) in HeLa cells. HeLa cells were pretreated with 10 mM sodium chlorate for 24 h before virus infection as indicated. Cells were harvested for whole-cell extract preparation and Western blotting to detect RSV P protein, HPIV3 HN protein, and ZIKV ENV protein, separately. (F) Role of PAPS synthases in EV71 replication. The HeLa WT cells, the PAPSS1 and PAPSS2 double-KO cells, and the reconstituted cells as indicated were infected with EV71 at an MOI of 0.1. The cells were harvested at 24 hpi for whole-cell extract preparation and Western blotting to detect EV71 VP1 protein.  $\alpha$ -Tubulin was used as an internal control. The expression levels of PAPSS1 and PAPSS2 were detected by endogenous antibodies (PAPSS1 and PAPSS2) and anti-Flag tag antibody. (G) Alignment of the nucleic acid sequences of the double-KO clone of PAPSS1 and PAPSS2 with HeLa WT cells by Sanger sequencing. The sgRNA targeting sites are highlighted in red. The red dashes indicate deleted bases, the black triangle indicates the inserted site in the KO clone, and the inserted bases are shown in blue lettering below the sequence. The PAM site is marked in green lettering. (H and I) CCK-8 cytotoxicity assay in HeLa cells or RD cells. Cells were seeded into a 96-well plate and incubated with different concentrations of sodium chlorate for 24 h, followed by the addition of 10  $\mu\text{L}$  of the CCK-8 solution to each well and incubation for 2 h in the incubator (at 37°C and 5%  $\text{CO}_2$ ). The absorbance at 450 nm was measured using a microplate reader. Experiments were repeated three times, and results are presented as the mean  $\pm$  SD.

of RD cells grown in a medium containing 0 to 30 mM sodium chlorate. Similarly, the VP1 reduction levels were proportional to the concentrations of sodium chlorate added in the immunoblotting assay (Fig. 5D). The CCK-8 assay revealed that sodium chlorate had minimal cytotoxicity at 10 mM (Fig. 5I).

As a bifunctional enzyme, 3'-phosphoadenosine 5'-phosphosulfate synthase (PAPSS) with both ATP sulfurylase and APS kinase activity mediates two steps in the sulfate activation pathway. In humans, there are two isoforms of PAPSS, PAPSS1 and PAPSS2. They are responsible for synthesizing PAPS from ATP and inorganic sulfate. As the sole source of sulfate, PAPS is the universal sulfur donor for all sulfotransferases in mammals. To further confirm that host sulfation was required for EV71, we generated a PAPSS1 and PAPSS2 double-knockout (DKO) clone by CRISPR-Cas9 technology. Sequencing showed that the selected clone had indels (a noninteger multiple of three) in the coding regions of the targeted gene (Fig. 5G), and immunoblotting using corresponding endogenous antibodies confirmed that both the PAPSS1 and PAPSS2 proteins were not expressed in the KO cells. The double knockout of the PAPSS1 and PAPSS2 genes significantly inhibited EV71 replication. Simultaneously, rescue assays for the ectopic expression of PAPSS1 and/or PAPSS2 in double-knockout clones resulted in the complete recovery of EV71 replication (Fig. 5F). This result indicated that the two genes, PAPSS1 and PAPSS2, had the same function. The inactivation of one of these genes had little or no effect on the biological phenotype. The result also explained why the sgRNAs of either PAPSS1 or PAPSS2 were not enriched in the CRISPR screens.

**Heparan sulfate is required for EV71 infection.** HS was reported to act as an important attachment receptor for EV71 (9). Our study's findings verify this result. According to our screening results, multiple genes involved in HS biosynthesis and sulfation pathways are highly enriched after EV71 infection. B3GAT3 is one of the various glycosyltransferases required for the synthesis of the backbones of HS. In comparison, SLC35B2 is responsible for sulfation modification at specific positions after the synthesis of the sugar backbone of HS. In addition to the sulfation of HS, SLC35B2 participates in another sulfation pathway: protein tyrosine sulfation. We found stronger resistance against EV71 in SLC35B2<sup>KO</sup> cells than in B3GAT3<sup>KO</sup> cells. However, it was unclear which sulfation pathway contributes to EV71 infection. To determine whether heparan sulfate on the cell surface played a significant role in virus-receptor interactions, various concentrations of heparin, a sulfated heparan sulfate analog, were preincubated with EV71 before the infection of HeLa cells. The viral protein VP1 was measured at 24 hpi via a Western blot assay. Significant inhibition of EV71 by heparin was observed only at concentrations above 500  $\mu\text{g}/\text{mL}$  (Fig. 6A). A similar inhibitory trend was observed in the evaluated RD cells (Fig. 6F). The preincubation of HeLa and RD cells with heparin at concentrations ranging from 100 to 1,000  $\mu\text{g}/\text{mL}$  before viral infection had no inhibitory effect but enhanced virus infectivity (Fig. 6B and G). These results demonstrate that the inhibitory effect is due to the direct interaction of heparin with EV71 and not with the target cells.

To further confirm the significance of HS on the cell surface, we tested the infectivity of EV71 for cells pretreated with heparinase II, which can degrade both heparin and heparan sulfate. The treatment of WT cells with each of the heparinases at 3 mIU/mL and 6 mIU/mL was found to significantly reduce the viral protein VP1 levels at 24 hpi (Fig. 6C and H). There was little change in the levels of EV71 infection for the SLC35B2<sup>KO</sup> clone with the same enzymatic removal of HS from the cell surface; the change was not nearly to the extent observed for the HeLa and RD WT cells. These data collectively revealed that HS played an essential role in EV71 infection.

Next, we reintroduced various concentrations of heparin in WT cells and SLC35B2<sup>KO</sup> cells pretreated with heparinase II at 3 mIU/mL. Consistent with the above observation, pretreatment with heparin at concentrations ranging from 0 to 500  $\mu\text{g}/\text{mL}$  before viral infection could significantly enhance the viral infectivity for WT cells in a dose-dependent manner (Fig. 6D and I) but not for the SLC35B2<sup>KO</sup> clone (Fig. 6E and J). This result



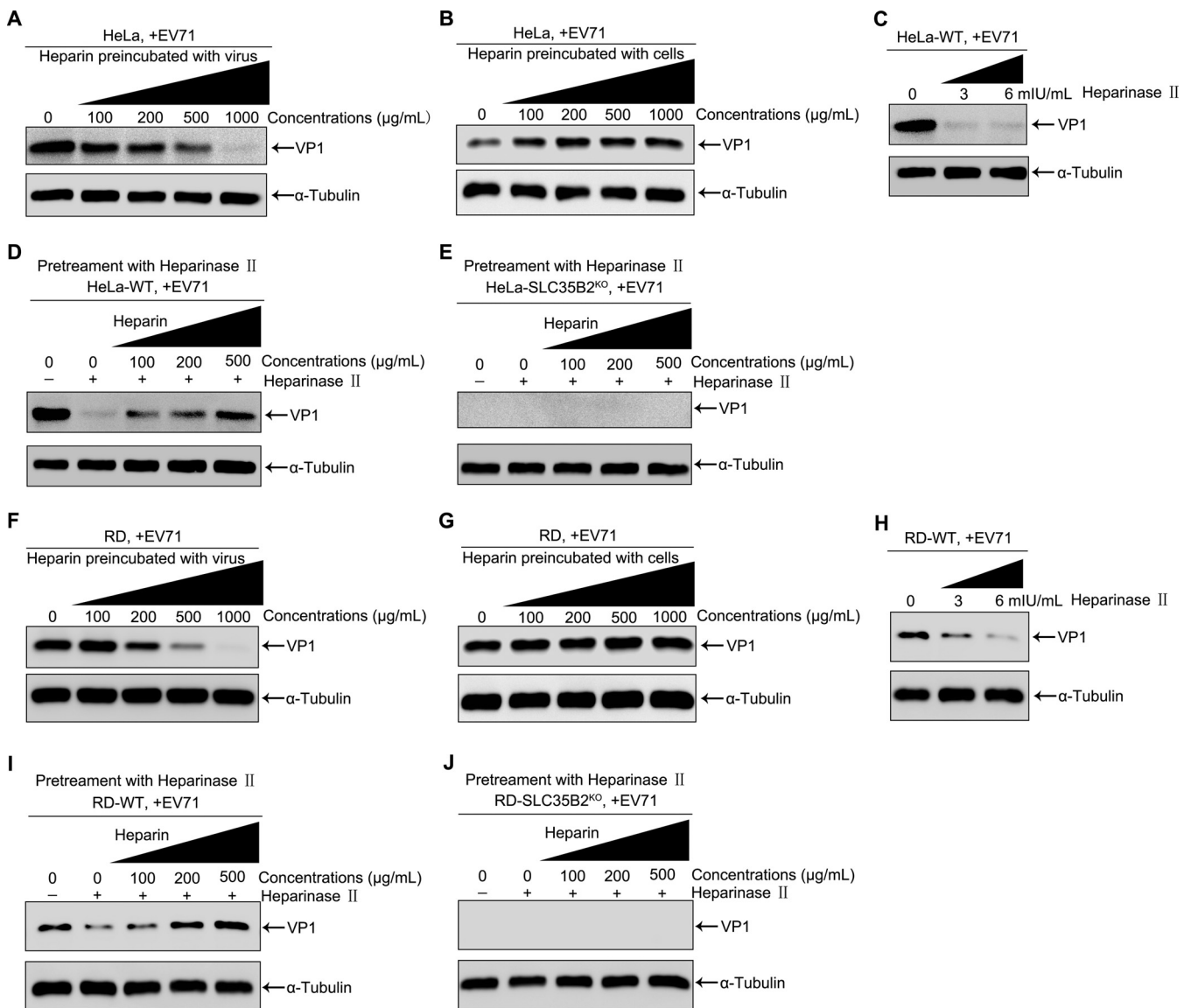


**FIG 6** Heparan sulfate is required for EV71 infection. (A and F) For the viral inactivation assay, various concentrations of heparin (0, 100, 200, 500, 1,000  $\mu\text{g/mL}$ ) were preincubated with EV71 for 1 h at 37°C before infection of HeLa cells (A) and RD cells (F). Following incubation for 2 h, cells were washed with PBS and cultured for 24 h in fresh complete DMEM. Cells were harvested at 24 hpi for whole-cell extract preparation and Western blotting to detect EV71 VP1 protein.  $\alpha$ -Tubulin was used as an internal control. (B and G) For the cell protection assay, various concentrations of heparin (0, 100, 200, 500, 1,000  $\mu\text{g/mL}$ ) were preincubated with HeLa cells (B) and RD cells (G) for 1 h at 37°C before EV71 infection. Following incubation for 2 h, cells were washed with PBS and cultured for 24 h in fresh complete DMEM. Cells were harvested at 24 hpi for whole-cell extract preparation and Western blotting to detect EV71 VP1 protein.  $\alpha$ -Tubulin was used as an internal control. (C and H) Inhibitory effects of heparinase II on EV71 infection. HeLa cells (C) and RD cells (H) were pretreated with various concentrations of heparinase II (0, 3, and 6 mIU/mL) for 1 h at 37°C before EV71 infection at an MOI of 0.1. Following incubation for 2 h, cells were washed with PBS and cultured for 24 h in fresh complete DMEM. Cells were harvested at 24 hpi for whole-cell extract preparation and Western blotting to detect EV71 VP1 protein.  $\alpha$ -Tubulin was used as an internal control. (D, E, I, and J) Add-back assay for heparin in HeLa WT cells (D), RD WT cells (I), HeLa SLC35B2<sup>KO</sup> cells (E), and RD SLC35B2<sup>KO</sup> cells (J). Cells were first pretreated with 3 mIU/mL heparinase II for 1 h at 37°C and then washed with PBS. After removal of the heparan sulfate on the cell surface, the cells were treated with heparin at 37°C for 1 h, thoroughly washed with PBS twice, and infected with EV71 at an MOI of 0.1. The cells were harvested at 24 hpi for whole-cell extract preparation and Western blotting to detect EV71 VP1 protein.  $\alpha$ -Tubulin was used as an internal control.

indicated that besides HS, some sulfated proteins are dependent on SLC35B2 and involved in EV71 entry.

**Sulfated proteins, in addition to heparan sulfate, are involved in EV71 entry.** To explore whether protein tyrosine sulfation affected EV71 infection, we generated a TPST1 and TPST2 double-knockout (DKO) clone using the CRISPR-Cas9 system. Sequencing showed that the selected clone had indels in the coding regions of the targeted gene (a noninteger multiple of three) (Fig. 7A). In agreement with the results above, the double

knockout of the TPST1 and TPST2 genes significantly inhibited EV71 replication, with less VP1 detected in the DKO cells than in the WT cells at 24 hpi (Fig. 7B).

As protein tyrosine sulfation is catalyzed by TPST through the transfer of a sulfate group from PAPS to tyrosine residues in a variety of proteins (including secretory proteins, plasma membrane proteins, and lysosomal proteins), we speculated that for a protein to be sulfated, it must derive from secretory or membrane proteins and proximate to TPST. TPST is located only in the trans-Golgi. Thus, we focused on secretory or membrane proteins that can be posttranslationally modified in the Golgi apparatus. We hypothesized that tyrosine-sulfated proteins must be found in the Golgi apparatus. There might be colocalization and interaction of sulfated proteins and TPSTs. The known protein receptors for EV71 were therefore investigated using coimmunoprecipitation (Co-IP) assays. As shown in Fig. 7C and D, SCARB2 can interact with TPST1 and TPST2 regardless of whether SCARB2 or TPST1/TPST2 is immunoprecipitated. In contrast, other proteinaceous receptors for EV71, including NCL, VIM, and ANX2, could not interact with TPST1 or TPST2 (Fig. 7E to I). Simultaneously, PSGL-1 and CCR5, which are two known viral receptors with tyrosine sulfation, were used as positive controls (Fig. 7E and F). These Co-IP assays showed that SCARB2 specifically interacted with TPSTs, which implied that SCARB2 might be sulfated.

**SCARB2 can be sulfated, and its tyrosine sulfation is critical for EV71 replication.**

Next, we performed computational prediction of sulfation sites and observed several tyrosine-sulfated sites on SCARB2: Y213 (SVM [support vector machine] probability of 0.72) and Y284 (SVM probability of 0.57) using a new version of SulfoSite and Y284, Y343, and Y388 using the older version of SulfoSite. By using GPS-TSP 1.0 to predict sulfation sites on SCARB2, Y284 (score = 1.228) was also predicted. In addition, Y213 (score = 0.955) and Y222 (score = 1.436) were obtained.

To verify these predicted tyrosine-sulfated sites, we then employed a liquid chromatography-tandem mass spectrometry (LC-MS/MS) approach on a Q Exactive HF-X mass spectrometer to analyze the potential tyrosine-sulfated sites of SCARB2. Two tagged SCARB2 samples (Flag and Myc, respectively) were immunoprecipitated using corresponding antitag beads, and then mass spectrometry-based methods for the study of tyrosine sulfation were performed (Fig. 8A, top). Five tyrosine-sulfated residues were identified in total (Fig. 8A, bottom): Y7, Y198, Y267, Y284, and Y410. Y284 might be a well-modified site on SCARB2 that can be both detected by mass spectrometric analysis and predicted by two different predictors of tyrosine-sulfated sites.

To test the actual biological functions of potential tyrosine-sulfated sites, we first constructed a series of SCARB2 mutants with one or more tyrosine-to-phenylalanine (Y-to-F) substitutions, which prevent tyrosine sulfation. Then, we transfected SCARB2-deficient HeLa cells with these SCARB2 mutants. At 24 h posttransfection, we then infected cells with EV71 at an MOI of 0.1. Finally, Western blot analysis indicated that the substitution of any one of these five tyrosine sites fully restored (Y7F, Y198F, Y267F, Y284F, or Y410F) the susceptibility of mutant SCARB2 to EV71 under the condition of the same expression as WT SCARB2 (Fig. 8B, lanes 3 to 8). The substitution of four tyrosine sites (Y198F, Y267F, Y284F, and Y410F; i.e., SCARB2-4YF or B2-4YF) also conferred a similar EV71 infectivity (Fig. 8B, lane 9). Simultaneous site-directed mutagenesis at these five tyrosine-sulfated sites (Y7F, Y198F, Y267F, Y284F, and Y410F; i.e., SCARB2-5YF or B2-5YF) also significantly, or even completely, recovered EV71 infection in SCARB2-deficient cells (Fig. 8B, lane 10). Only the mutant with all 20 tyrosine residue substitutions (i.e., SCARB2-20YF or B2-20YF) could not recover the EV71 infectivity at all in SCARB2-deficient cells, as shown by the complete lack of detection of viral protein using Western blot analysis (Fig. 8B, lane 11). Similar transient-transfection experiments were conducted in another cell line, RD, and we obtained similar results (Fig. 8D). Subsequently, we performed rescue assays by the retroviral expression of C-terminally Flag-tagged SCARB2 mutants with phenylalanine substitutions in SCARB2-deficient HeLa and RD cells. We found that the knockout of SCARB2 significantly inhibited EV71 infection, and the ectopic expression of the WT SCARB2 and the SCARB2-4YF and

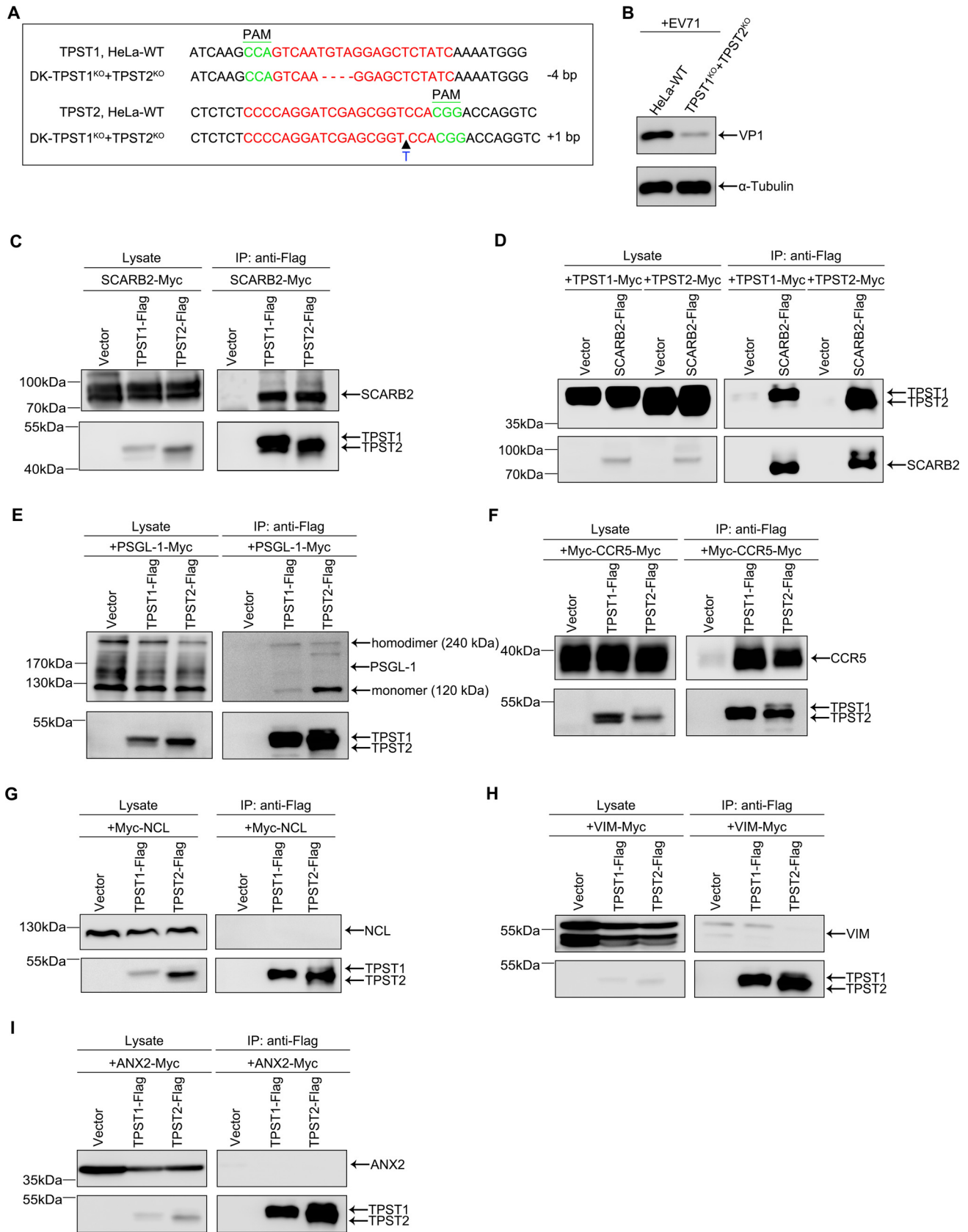


**FIG 7** Tyrosine-sulfated proteins, in addition to heparan sulfate, are involved in EV71 entry. (A) Alignment of the nucleic acid sequences of double-KO clone of TPST1 and TPST2 with HeLa WT cells by Sanger sequencing. The sgRNA targeting sites are highlighted in red. Red dashes indicate deleted (Continued on next page)

SCARB2-5YF mutants in the corresponding KO cells resulted in the complete recovery of EV71 replication. However, the SCARB2-20YF mutant failed to restore any susceptibility to EV71, consistent with the results from transient-transfection experiments (Fig. 8C and E). To exclude the influence of point mutations on protein structure, we performed a series of Co-IP assays. As shown in Fig. 8F and G, SCARB2, SCARB2-5YF, and SCARB2-20YF could interact with TPST1 and TPST2. Then, we introduced another known interaction between SCARB2 and beta-glucocerebrosidase (GBA) (69) to test whether SCARB2 mutants could interact with GBA. As shown in Fig. 8H, SCARB2-5YF and SCARB2-20YF could also interact with GBA. These Co-IP results indicate that those point mutations of tyrosine to phenylalanine are unlikely to result in a conformational change of SCARB2. In addition, we overexpressed the empty vector and Myc-tagged or Flag-tagged SCARB2-WT, SCARB2-5YF, and SCARB2-20YF plasmids in HeLa cells. At 24 hpt, cells were analyzed by fluorescence microscopy. The immunofluorescence data showed that the localization of SCARB2 mutants was not significantly altered compared to that of SCARB2-WT, which was consistent with the data obtained using coimmunoprecipitation (data not shown).

To conclude, these results demonstrate that SCARB2 can be sulfated at multiple tyrosine residues beyond five identified tyrosine residues (Y7, Y198, Y267, Y284, and Y410) and that this tyrosine sulfation is critical for EV71 infection. Hence, the exact tyrosine-sulfated sites and the spatial-temporal regulation of SCARB2 remain to be determined.

## DISCUSSION

As an obligate intracellular pathogen, EV71 depends on various cellular factors to complete its life cycle. During EV71 infection, viral entry is an initial and multistep process, including binding, internalization, and uncoating. The first step is binding to receptors expressed on the surfaces of susceptible cells, which is the key to establishing effective infection and determines the cell or tissue tropism of EV71. More than 10 molecules have so far been reported to act as possible receptors that facilitate EV71 infection. Except for PSGL-1 and SCARB2, which are the two best-characterized receptors for EV71, other receptors, including ANX2, VIM, NCL, HSPG, sialylated glycan, DC-SIGN, prohibitin, and fibronectin, are not well characterized and require additional evidence and research for support. Despite multiple receptors available for EV71, the actual pattern of usage needs to be elucidated. In other words, we need to know the following issues, including which receptor binds to virions in the first place and which receptor binds later, which receptor mediates attachment and internalization, and which receptor mediates uncoating. The interrelationship is competitive inhibition or collaborative enhancement among these receptors. In addition, the knowledge of EV71 replication and its infection-induced pathogenesis is still limited. Thus, it is meaningful that we conducted a pooled, unbiased genome-wide CRISPR-Cas9 knockout screen (with virus-induced cell death readout phenotypes) to investigate EV71 for the first time.

In this study, for the first time, we conducted a pooled, unbiased genome-wide CRISPR-Cas9 knockout screen (with virus-induced cell-death readout phenotypes to investigate EV71) and identified a set of host factors which are critical for EV71 infection (Fig. 1B; see Table S1 in the supplemental material). Several studies have indicated that SCARB2 can facil-

### FIG 7 Legend (Continued)

bases, the black triangle indicates the inserted site in the KO clone, and the inserted bases are shown in blue lettering below the sequence. The PAM site is displayed in green lettering. (B) Evaluation of the role of tyrosyl protein sulfotransferase in EV71 replication. The HeLa WT clone and the TPST1 and TPST2 double-KO clone were infected with EV71 at an MOI of 0.1. Western blot analysis of viral protein levels is shown.  $\alpha$ -Tubulin was used as an internal control. (C and D) Coimmunoprecipitation assay to investigate the TPST1- or TPST2-SCARB2 interaction. HEK293T cells were transfected with the indicated plasmids. The cells were harvested at 48 h posttransfection and subjected to immunoprecipitation (IP) using an anti-Flag affinity gel. The immunoprecipitates and input samples were analyzed by Western blotting using the indicated antibodies (anti-Flag and anti-Myc). (E to I) Coimmunoprecipitation assay to investigate the TPST1- or TPST2-PSGL-1 interaction (E), the TPST1- or TPST2-CCR5 interaction (F), the TPST1- or TPST2-NCL interaction (G), the TPST1- or TPST2-VIM interaction (H), and the TPST1- or TPST2-ANX2 interaction (I). HEK293T cells were transfected with the indicated plasmids. The cells were harvested at 48 h posttransfection and subjected to IP using anti-Flag affinity gel. The immunoprecipitates and input samples were analyzed by Western blotting using the indicated antibodies (anti-Flag and anti-Myc).

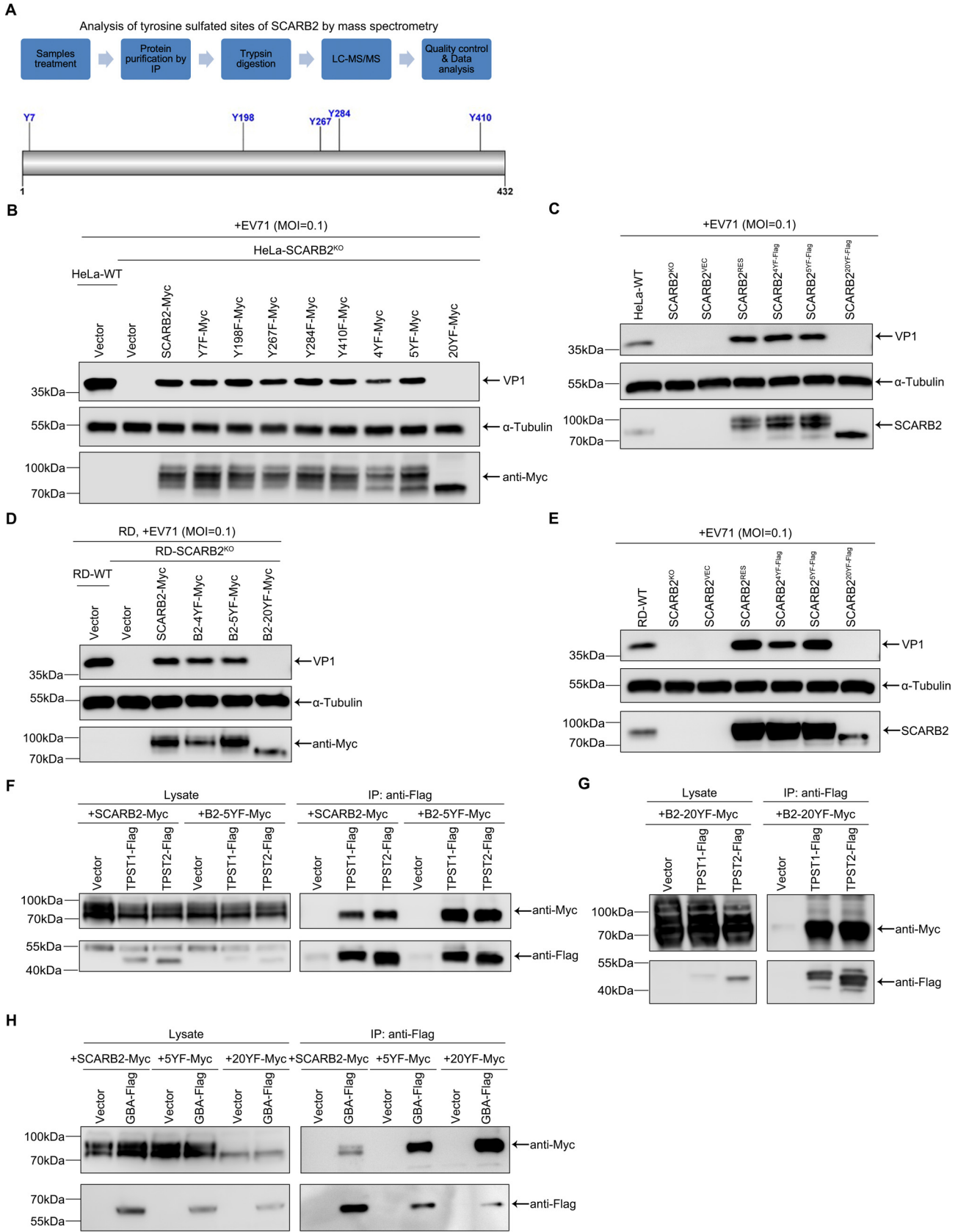


**FIG 8** SCARB2 can be sulfated, and its tyrosine sulfation is critical for EV71 replication. (A) Mass spectrometry to identify protein tyrosine sulfation. pCAGGS-SCARB2-Myc was transfected into HEK293T cells. The cells were harvested at 48 h posttransfection and subjected to immunoprecipitation (Continued on next page)

itate efficient EV71 infection by playing critical roles in viral binding, internalization, and uncoating (70–72). Consistently, among the candidate genes, SCARB2 was ranked first in the positive selection, with all three separate sgRNAs highly enriched (Fig. 1F). Furthermore, HSPG has been identified as an attachment receptor essential for EV71 infection (9). This finding was not achieved through large-scale genetic screening but is based on two known findings, i.e., that EV71 has a wide range of tissue tropisms and that HSPGs are ubiquitously expressed by most cell types. Hence, the researchers speculated that EV71 infection might be facilitated by using expressed heparan sulfate as an attachment receptor. Although the study showed that HSPG inhibition resulted in inhibition of EV71 infection in RD cells, the exact mechanism of HSPG that promotes EV71 infection remained unclear. Consistent with this study, our screening result showed that multiple HSPG-related genes were highly enriched, including B3GAT3, XYLT2, FAM20B, B3GALT6, and B4GALT7, which are involved in the biosynthesis of glycosaminoglycans. Additionally, two genes, HS6ST1 and SLC35B2, were responsible for the sulfation of GAGs (Fig. 1C and Table S1). As expected, the knockout of B3GAT3 or SLC35B2 dramatically inhibited EV71 replication (Fig. 2 and 3). Our results support a critical role for HSPGs in both RD and HeLa cells. These data collectively imply that our screening process for EV71 was effective and reasonable.

B3GAT3 and XYLT2 encode enzymes responsible for HSPG synthesis, whereas SLC35B2 encodes a PAPS transporter that mediates the delivery of the universal sulfate donor, PAPS, from the cytosol, where it is synthesized, into the Golgi lumen, where sulfation events occur. Although SCARB2 and B3GAT3 are well characterized, the role of SLC35B2 and the interrelationships between SLC35B2 and SCARB2 or B3GAT3 during EV71 infection require further elucidation. To this end, we first generated individual KO clones for SCARB2, SLC35B2, and B3GAT3 in both the HeLa and RD cell lines and examined the requirements for EV71 infection. Western blot and RT-qPCR analyses revealed that the knockout of any one of these three genes significantly inhibited EV71 replication (Fig. 2). We must point out that RT-qPCR analyses (Fig. 2B and F) provided more helpful information than Western blot analyses (Fig. 2C and G). At 2, 6, 12, and 24 hpi, viral proteins in all three KO clones were detectable, showing no difference. However, RT-qPCR analyses showed a differential and quantitative change in the viral RNA levels of these three KO clones. Specifically, at 2 hpi, knockout of SLC35B2 or B3GAT3 showed a significant reduction in the viral RNA levels, whereas knockout of SCARB2 did not influence the viral level to the same extent as the RNA level in WT cells. Notably, at 12 and 24 hpi, knockout of SCARB2 conferred the most robust resistance against EV71 infection, with an ~1,000-fold reduction in the viral RNA level. In contrast, the knockout of SLC35B2 and B3GAT3 showed a moderate reduction in viral RNA levels. At 6 hpi, SCARB2 knockout showed a different effect on EV71 infection between HeLa and RD cells. In HeLa cells, all three KO clones had a similarly reduced level of EV71 infection, while in RD cells, knockout of SCARB2 resulted in moderate-level protection against EV71. This phenomenon could be explained by the varying sensitivity to EV71 of different cell lines

#### FIG 8 Legend (Continued)

using anti-Myc affinity gel. Then, bead samples were incubated in the reaction buffer at 95°C for 10 min for protein denaturation, cysteine reduction, and alkylation. The eluates were subjected to trypsin digestion overnight at 37°C by adding 1 μg of trypsin. The peptides were purified using desalting columns. The resulting tryptic peptides were analyzed on a Q Exactive HF-X mass spectrometer coupled with an Easy-nLC 1200 system (Thermo Scientific). (Top) Flow chart of analysis of tyrosine-sulfated sites of SCARB2 by MS. (Bottom) Five tyrosine residues (Y7, Y198, Y267, Y284, and Y410) were identified as sulfation sites. (B and D) Rescue assay for the transient expression of C-terminally Myc-tagged SCARB2 mutants with phenylalanine substitutions in HeLa or RD SCARB2<sup>KO</sup> cells. A series of SCARB2 mutants were constructed and transfected into SCARB2<sup>KO</sup> cells. Four hours after transfection, cells were inoculated with EV71 at an MOI of 0.1. The cells were harvested at 24 hpi or 12 hpi for whole-cell extract preparation and Western blotting to detect EV71 VP1 protein. α-Tubulin was used as an internal control. 4YF (SCARB2-4YF) refers to the SCARB2 mutant with four tyrosine-to-phenylalanine substitutions, including Y198F, Y267F, Y284F, and Y410F. 5YF (SCARB2-5YF) refers to the SCARB2 mutant with five tyrosine-to-phenylalanine substitutions, including Y7F, Y198F, Y267F, Y284F, and Y410F. 20YF (SCARB2-20YF) refers to the SCARB2 mutant with 20 tyrosine-to-phenylalanine substitutions. Here, some SCARB2 designations are abbreviated to B2. (C and E) Rescue assay for the retroviral expression of C-terminally Flag-tagged SCARB2 mutants with phenylalanine substitutions in HeLa or RD SCARB2<sup>KO</sup> cells. A series of SCARB2 mutants were cloned in the lentiviral expression vector. After packaging of the corresponding lentiviruses, the stable cell lines for the retroviral expression of C-terminally Flag-tagged SCARB2 mutants were constructed into the SCARB2<sup>KO</sup> clone and screened by blasticidin (10 μg/mL). Then, EV71 was inoculated into cells stably transfected with SCARB2 tyrosine-sulfated mutants at an MOI of 0.1. The cells were harvested at 24 or 12 hpi for whole-cell extract preparation and Western blotting to detect EV71 VP1 protein. α-Tubulin was probed as an internal control. (F to H) Coimmunoprecipitation assay to investigate the interactions between TPST1, TPST2, or GBA and SCARB2 and its mutants. HEK293T cells were transfected with the indicated plasmids. The cells were harvested at 48 hpi and subjected to immunoprecipitation (IP) using anti-Flag affinity gel. The immunoprecipitates and input samples were analyzed by Western blotting using the indicated antibodies (anti-Flag and anti-Myc).

and potential experimental errors. These RT-qPCR results suggested that SCARB2 may play a critical role 2 h later after EV71 challenge. Typically, viral entry occurs within 30 min in highly permissive cells. We consequently speculated that SCARB2 was critical for EV71 entry, specifically uncoating, rather than binding and internalization.

After the functional validation experiments, we attempted to determine whether these genes functioned in distinct virus entry stages, including binding, internalization, and uncoating; a variety of methods were applied. Binding assays based on RT-qPCR (Fig. 4A and B), immunofluorescence (Fig. 4C), and flow cytometric analyses (Fig. 4G) produced similar results: the knockout of the SLC35B2 or B3GAT3 gene resulted in a significant reduction in the EV71-binding capacity compared to that of WT cells, whereas the knockout of the SCARB2 gene did not affect EV71 attachment. Internalization assays based on RT-qPCR (Fig. 4D and E) and immunofluorescence (Fig. 4F) showed that knockout of SLC35B2 and B3GAT3, but not SCARB2, significantly reduced EV71 internalization into HeLa and RD cells. To further confirm that SLC35B2 or B3GAT3 played an essential role in the EV71 entry step rather than other later steps during virus infection, we transfected EV71 RNAs transcribed *in vitro* into WT cells and the corresponding KO cells. We observed not only no obvious cytopathic effects (CPEs) from EV71 at 48 hpt but also no statistically significant differences in the cytoplasmic expression levels of viral RNAs between individual KO and WT cells by RT-qPCR analysis at 12 hpt (Fig. 4H and I). This indicated that the loss of SLC35B2, or B3GAT3, did not affect the following steps of EV71 replication after viral RNAs are transported into the cytosol. We did not provide direct evidence for SCARB2 acting as an uncoating receptor for EV71, but we could infer from all the data above that the knockout of SCARB2 affects EV71 infection at 2 to 6 hpi (after internalization but before genome RNA replication). This time frame exactly corresponds to the uncoating step, which is in line with the observation that capsid was barely detected after 4 h postinfection (72). Collectively, we demonstrated that SLC35B2 and B3GAT3 are essential for EV71 attachment and internalization, while SCARB2 may play a critical role in the subsequent step, uncoating. Our results suggest that SCARB2 is not responsible for the initial binding and internalization, which appears to contradict some previous findings that SCARB2 is an attachment receptor for EV71 (4, 73). Our finding can be rationalized by comparing the amounts of SCARB2 in different cellular locations. Obviously, the majority of SCARB2 is localized in the lysosomal membrane (74). In contrast, only a tiny amount of SCARB2 may shuttle to the plasma membrane. Compared with the large number of HSPGs on the cell surface, the role of SCARB2 on the cell surface in binding and internalization can be ignored. In addition, a study by Du et al. provided some support for this idea (8). However, this does not mean that SCARB2 is not required for efficient viral entry. On the contrary, as the only known uncoating receptor, SCARB2 probably plays an essential role in the uncoating step but a minimal role in attachment or internalization during EV71 entry. Therefore, effective EV71 infection depends on both HS and SCARB2, which act together and cooperatively to facilitate EV71 entry.

Next, <sup>35</sup>S isotope labeling was conducted to demonstrate the vital role of SLC35B2 in regulating host cell sulfation. As shown in Fig. 5A and B, a functional PAPST1, but not an enzymatically inactive mutant, was important for allowing sulfation of cellular proteoglycans and proteins, which is in line with a previous study (67). To further confirm the significance of sulfation for EV71 infection, an ATP-sulfurylase inhibitor, sodium chlorate, was used. We found that the EV71 RNA levels were inversely proportional to the concentrations of sodium chlorate added (Fig. 5C and D). Interestingly, Hallak et al. demonstrated that glycosaminoglycan sulfation is important for RSV infection (75). Our sodium chlorate inhibitory experiments consistently supported this finding (Fig. 5E). In addition, PAPS biosynthesis by knocking out two synthetases, PAPSS1 and PAPSS2, significantly reduced EV71 infection in HeLa cells (Fig. 5F). As reported, there are two main types of sulfation: the sulfation of proteoglycans and the sulfation of secretory or membrane proteins. Consistent with previous findings on the role of heparan sulfate in binding to EV71 (9), heparin inhibited EV71 infection in a concentration-dependent manner (Fig. 6A and F).

Furthermore, the enzymatic removal of heparan sulfate by heparinase II also inhibits EV71 infection (Fig. 6C and H). When we reintroduced exogenous heparin in WT cells after the removal of the cell surface heparan sulfate by heparinase II, heparin promoted EV71 infection in a concentration-dependent manner (Fig. 6D and I). However, no significant infection was detected in the SLC35B2<sup>KO</sup> cells under the same conditions (Fig. 6E and J). These data not only support the idea that heparan sulfate is an important attachment receptor for EV71 but also indicate that sulfated proteins other than those that are sulfation modified with heparan sulfate are deficient in the SLC35B2<sup>KO</sup> clone and may contribute to EV71 entry. To validate this hypothesis, we generated a double-knockout clone for TPST1 and TPST2. The loss of TPST1 and TPST2 resulted in strong resistance against EV71 infection (Fig. 7B). Then, we screened some proteins to investigate whether an interaction occurred between them and TPSTs. CCR5 and PSGL-1 were found to be sulfated at multiple tyrosine sites and were included as positive controls. Finally, among the receptors for EV71, we identified that SCARB2 could interact with TPSTs (Fig. 7C and D), which implies the existence of tyrosine sulfation on SCARB2. Since most tyrosine sulfation occurs on proteins that are secreted or membrane bound, it is no surprise that SCARB2, as one of the most abundant lysosomal membrane proteins, has the potential to be sulfated. Furthermore, we identified five potential tyrosine-sulfated sites on SCARB2 by mass spectrometry (Fig. 8A). In complementary experiments, the reconstitution of the SCARB2 mutant with these five tyrosine residues replaced with phenylalanine residues in SCARB2-deficient cells fully recovered the susceptibility to EV71 infection, whereas the reconstitution of the mutant with all the tyrosine residues replaced with phenylalanine residues could not recover the susceptibility at all (Fig. 8B to E). This implies that there are unidentified tyrosine-sulfated sites other than these five sites on SCARB2. Except for SCARB2, we are unsure whether other sulfated proteins are associated with EV71 infection. A systematic screening method must be developed to identify candidate proteins that can be sulfated. TPST substrates containing multiple tyrosine-sulfated sites are common. For the chemokine receptor CCR5, four sulfated tyrosine residues (Y3, Y10, Y14, and Y15) located in the N-terminal extracellular region were shown to be crucial in mediating HIV binding and infection (52, 76). For PSGL-1, three potential tyrosine residues (Y46, Y48, and Y51) in the amino terminus of PSGL-1 can be sulfated, but only the sulfation of Y48 and Y51 may be critical for EV71 binding and infection (19). Our results presented in this study reveal a different tyrosine-sulfated pattern on SCARB2 from CCR5 and PSGL-1, whose tyrosine sulfation is in the amino-terminal region. Unlike CCR5 and PSGL-1, SCARB2 has a distinct tyrosine-sulfated pattern. In this study, we first discovered that SCARB2 is modified by tyrosine sulfation and proved that this atypical tyrosine sulfation is probably related to uncoating mediated by SCARB2. We provided some evidence to support the tyrosine sulfation of SCARB2, but we could not rule out the other potential sulfated proteins mediating EV71 entry and infection. Importantly, fibronectin was found to be tyrosine sulfated (77), and a recent study reported that fibronectin facilitates EV71 infection by mediating viral entry (13). However, we do not know whether the tyrosine sulfation of fibronectin is critical for EV71 infection. Therefore, the exact relationship between the sulfation of fibronectin and EV71 entry is under further investigation.

According to the overall results of this study, we constructed a schematic model of EV71 entry, as depicted in Fig. 9. Viral capsid proteins first bind to the attachment receptor, HSPGs, which possess heavily sulfated long GAG chains. Through electrostatic interactions with the basic residues of viral capsid proteins, EV71 virions are concentrated on the cell surface, thus augmenting the chance of binding a more specific entry receptor, such as SCARB2. The virus-receptor complex is subsequently internalized via endocytosis. Internalized viruses may encounter SCARB2 abundantly distributed in lysosomes or endosomes, where SCARB2 initiates a conformational change that leads to uncoating the virion at an acidic pH. Thus, EV71 completes all the steps of viral entry and releases its genomic RNA into the cytoplasm for a subsequent replication cycle. Briefly, SCARB2 and HSPG act sequentially and coordinately to mediate EV71 entry. The sulfation of HS and SCARB2 mediated by SLC35B2 is also important for the cell entry of



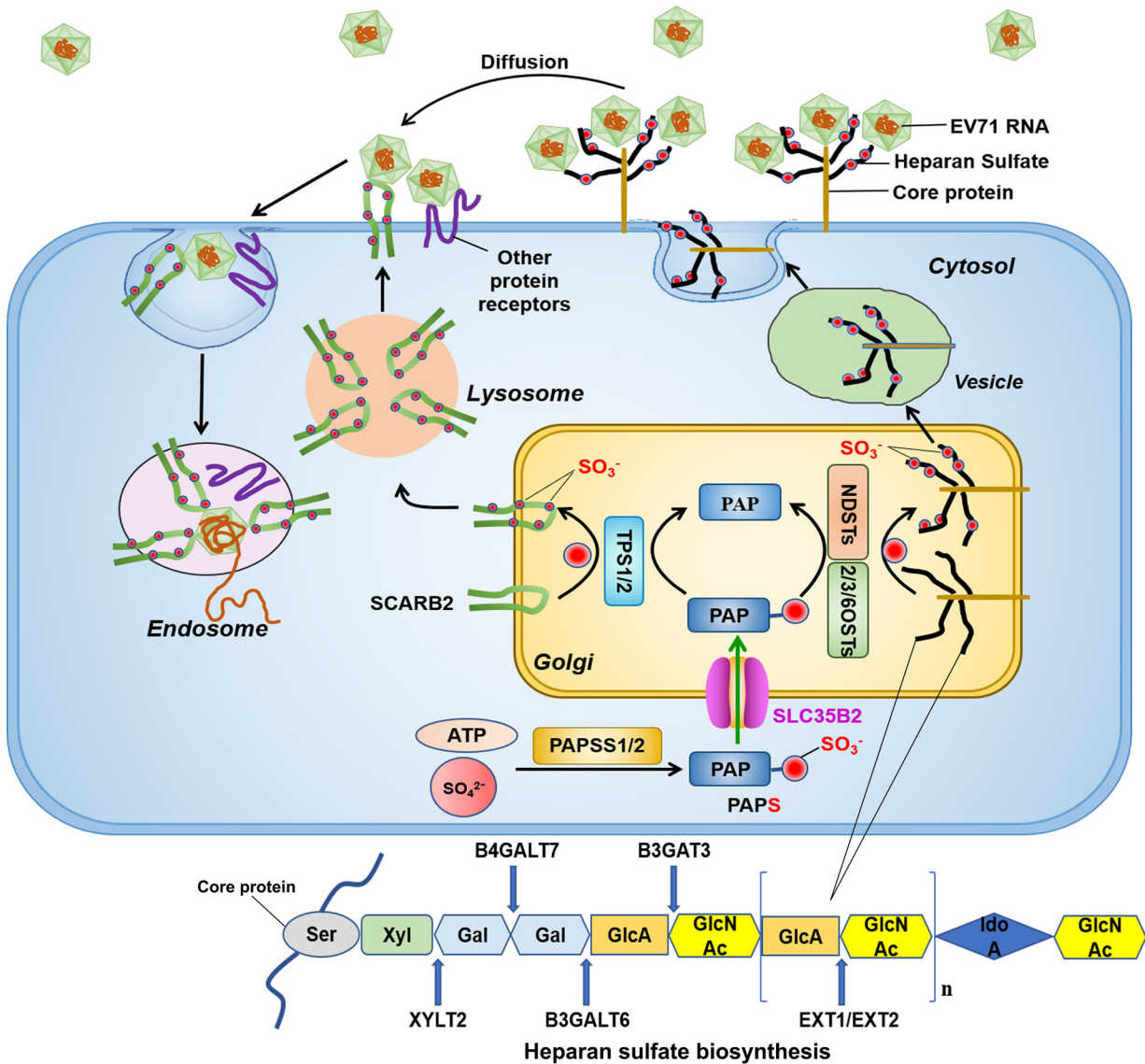


**FIG 9** Schematic representation of the entry model for EV71 infection. Schematically, to enter the target cells, viral capsid proteins first bind to the attachment receptor, heparan sulfate proteoglycan (HSPG), which possesses heavily sulfated long GAG chains. Through electrostatic interaction with the viral capsid proteins, EV71 virions are concentrated on the cell surface, thus augmenting the chance of binding a more specific entry receptor, such as SCARB2. The virus-receptor complex is subsequently internalized via endocytosis. Internalized viruses may encounter SCARB2 abundantly distributed in lysosomes or endosomes, where SCARB2 initiates a conformational change that leads to the uncoating of the virion under acidic conditions. Thus, EV71 completes all the steps of viral entry and releases its genomic RNA into the cytoplasm for a subsequent replication cycle. Briefly, SCARB2 and HSPG act sequentially and coordinately to mediate EV71 entry. The sulfation of HS and SCARB2 mediated by SLC35B2 is also important for the EV71 entry process. SLC35B2 has a dual function of mediating sulfation modification of glycosaminoglycans and proteins. Newly translated core proteins without HS chains and SCARB2 proteins are transported into the Golgi network. The biosynthesis of HSPG is initiated through the attachment of the first tetrasaccharide (GlcA-beta-1,3-Gal-beta-1,3-Gal-beta-1,4-Xyl) to a serine residue of the core protein and then the subsequent addition of *N*-acetylglucosamine (GlcNAc) and glucuronic acid (GlcA). There are four transferases involved in the linkage tetrasaccharide, including XYLT2 (xylosyltransferase 2), B4GALT7 (beta-1,4-galactosyltransferase 7), B3GALT6 (beta-1,3-galactosyltransferase 6), and B3GAT3 (beta-1,3-glucuronyltransferase 3), in sequential order. Then, HS polymerase EXT1/2 (exostosin glycosyltransferase 1/2) is involved in the chain elongation step of heparan sulfate biosynthesis. For HSPG sulfation, a series of sulfation modification reactions occur after HS chain formation, including *N*-sulfation, 2-*O*-sulfation, 3-*O*-sulfation, and 6-*O*-sulfation catalyzed by *N*-deacetylase/*N*-sulfotransferases (NDSTs), 2-*O*-sulfotransferase (2OST), 3OSTs, and 6OSTs, respectively. Sulfated heparan sulfate proteoglycans are then transported to the cell surface via secretory vesicles, acting as a major attachment receptor for EV71. For SCARB2 sulfation, TPST1 and TPST2 might be responsible for its specific tyrosine-sulfated pattern. Sulfated SCARB2 proteins are transported to lysosomes or endosomes. Only a small amount of the sulfated SCARB2 proteins continue to be transported to the cell surface, acting as a secondary attachment receptor for EV71. PAPS, 3'-phosphoadenosine-5'-phosphosulfate; Ser, serine, Xyl, xylose; Gal, galactose, GlcA, glucuronic acid; GlcNAc, *N*-acetylglucosamine; IdoA, iduronic acid.

EV71. SLC35B2 plays a dual function of mediating the sulfation modification of glycosaminoglycans and proteins. Newly translated core proteins without HS chains and SCARB2 proteins are transported into the Golgi network. For HSPG sulfation, a series of sulfation modification reactions occur after HS chain formation, including N-sulfation, 2-O-sulfation, 3-O-sulfation, and 6-O-sulfation, catalyzed by *N*-deacetylase/*N*-sulfotransferases (NDSTs), 2-O-sulfotransferase (2OST), 3OSTs, and 6OSTs, respectively. Sulfated heparan sulfate proteoglycans are then transported to the cell surface via secretory vesicles, acting as a major attachment receptor for EV71. For SCARB2 sulfation, TPST1 and TPST2 might be responsible for its specific tyrosine-sulfated pattern. Sulfated SCARB2 proteins are transported to lysosomes or endosomes. Only a tiny fraction of the sulfated SCARB2 proteins continues to be transported to the cell surface, acting as a secondary attachment receptor for EV71.

Of note, EV71 isolated from clinical samples is difficult to replicate in cultured cells. However, on the one hand, owing to their error-prone replication machinery, RNA viruses can rapidly mutate. On the other hand, HSPGs are abundantly expressed in most mammalian cells. A possible outcome is that EV71 viruses adapt to this cultured condition and replicate efficiently after a few passages. This results in improved viral fitness and the outcompeting of HSPG-independent variants. Tan et al. (78) reported that multiple lysine residues at positions 162, 242, and 244 of the VP1 capsid protein are responsible for electrostatic interaction with HS/heparin. In contrast, a double mutant (VP1-98E and VP1-145E) did not bind HS at all, although it acquired compensatory mutations (VP1-98K or VP1-145G/Q) rapidly, which restored HS binding. These results suggest that multiple positively charged residues around the 5-fold axis of EV71 capsid determine HS adaptation. Consistent with this, continuous passages of EV71 in cell culture often induce mutations in capsid proteins (79). Both VP1-98 and VP1-145 are HS/heparin-binding determinants and can modulate the positive charges at the 5-fold axis. The presence of VP1-98K creates a cluster of positive charges around VP1-K242, which could explain why mutants with VP1-K98 have restored HS/heparin binding. These results suggest that conversion from HS-nonbinding strains to HS-binding mutants is associated with adaptation of the virus to cell culture and that this occurs very frequently due to the abundant expression of HS on the surface of cultured cells. Kobayashi et al. (80) revealed that the HS-nonbinding mutant (VP1-145E) was more virulent than the HS-binding mutant (VP1-145G), by using human SCARB2-transgenic mice. Furthermore, this study suggested that the VP1-145G virus is attenuated by HS attachment receptor *in vivo*, leading to abortive infection of HS-positive cells. Fujii et al. (81) obtained similar results using cynomolgus monkeys. Tee et al. (82) generated multiple EV71 variants with various residues at VP1-98, VP1-145, and VP2-149 and showed that a weak heparin binder was highly lethal in mice. The initially strong heparin-binding variant acquired an additional mutation, which confers a weak heparin-binding phenotype and high virulence. More recently, another important paper from Kobayashi et al. (83) indicated that HS attachment receptor is an important selection factor for attenuated EV71 mutants at VP1-145 during cell culture adaptation. In this study, the EV71 strain we used was virus with the specific amino acid residues of VP1-97L, -98K, -145E, -167E, and -244K. Due to the presence of VP1-98K, the EV71 variant of our lab gained the ability to bind HS/heparin. As shown in Fig. 6A and F, heparin significantly inhibited EV71 infection of two cultured cell lines, HeLa and RD cells. Given the above, at least, HS might represent a promising antiviral target for preventing EV71 replication and dissemination.

Interestingly, during the study of the interaction of SLC35B2 and other proteins, we found that SLC35B2 can be oligomerized (data not shown). According to the UniProtKB sequence under accession no. [Q8TB61](#) (S35B2\_HUMAN), SLC35B2 has nine transmembrane (TM) regions. To test whether the oligomerization was important for EV71 infection, we generated SLC35B2 mutants with truncated TM regions. We found a functional oligopeptide ( $\Delta$ TM3–TM7, with TM3 to TM7 of SLC35B2 deleted) that retains the interaction with WT SLC35B2 but disturbs the ability to deliver PAPS. With the overexpression of this truncated mutant in HeLa WT cells, we observed significant inhibition against EV71 replication in a dose-dependent manner. Clausen et al. revealed HS as a novel attachment factor for

SARS-CoV-2 and suggested the possibility of using a sulfated heparan sulfate analog (such as heparin) (84). In addition, at least two genome-wide CRISPR screens have recently identified SLC35B2 as a host dependency factor critical for SARS-CoV-2 infection (85, 86). Based on our data and relevant literature, SLC35B2, as a broad-spectrum host factor essential for numerous viruses, may represent a more promising drug target than HS for fighting SARS-CoV-2 as well as EV71.

In conclusion, our research supports the previous findings of SCARB2 and HSPG acting as receptors for EV71. We also found that EV71 infection is codependent on heparan sulfate and SCARB2 and identified a new host factor, SLC35B2, which indirectly facilitates EV71 infection through regulation of the host cell sulfation, and determined a novel posttranslational modification, protein tyrosine sulfation, existing in SCARB2. Except for SCARB2, SLC35B2, and B3GAT3, our genetic screen yielded many other candidates that may be essential for EV71 infection and are worthy of being investigated.

## MATERIALS AND METHODS

**Cell lines.** Human embryonic kidney 293 cells that express a mutant version of the simian virus 40 (SV40) large T antigen (HEK293T), human rhabdomyosarcoma (RD) cells, human cervical cancer epithelial cells (HeLa), and HeLa derivative cells (Hep2) were obtained from the China Center for Type Culture Collection and were grown and maintained in Dulbecco's modified Eagle medium (DMEM) (Gibco) supplemented with 10% heat-inactivated fetal bovine serum (Newzerum) and 1% penicillin/streptomycin (catalog no. 15140122; Gibco).

**Plasmids, primers, chemicals, and reagents.** There were two lentiviral constructs in this study: lentiCRISPRv2 (catalog no. 52961; Addgene) and pCDH-CMV-IRES-MCS-SF-BLAST. psPAX2 (catalog no. 12260; Addgene) and PMD2.G (catalog no. 12259; Addgene) as a VSV-G envelope-expressing plasmid are used with lentiviral vectors to produce lentiviruses. The candidate genes and other related genes were cloned in the mammalian expression vector pCAGGS-MCS and/or pCDH-CMV-IRES-MCS-SF-BLAST. The primers were used as shown in Table S3 in the supplemental material.

The following chemicals and reagents were used in this study: heparin (catalog no. H3149; Sigma-Aldrich), sodium chlorate (catalog no. 403016; Sigma-Aldrich), and heparinase II (catalog no. 6336-GH; R&D).

**HeLa-GeCKO library generation and EV71 screen.** The HeLa-GeCKO library was generated using an all-in-one CRISPR-Cas9 vector system from Feng Zhang (human GeCKOv2 library; Addgene catalog no. 1000000048) as previously described (64). Briefly, we first used electrotransformation to amplify the ready-made sgRNA library and subsequently performed next-generation sequencing (NGS) to verify the quality of the amplified plasmid library. Second, the quantified plasmid library was cotransfected with lentiviral helper plasmids, pPMD2.G and psPAX2. After the lentivirus supernatant was harvested, HeLa cells were transduced with lentiviral sgRNA library (65,383 sgRNAs in total) at an MOI of <0.3 to attain no more than 1 sgRNA per cell and were selected with 1  $\mu$ g/mL puromycin for 10 days to generate the library cells. Finally, at least  $3.3 \times 10^7$  sgRNA library cells were mock infected (negative control) or infected with EV71 at an MOI of 0.1 in infection medium for 2 days in biological duplicates, and the surviving cells were allowed to expand. When the number of surviving cells reached  $\sim 3.3 \times 10^7$  (this cell number ensures over 500-fold coverage for an average sgRNA.), they were subjected to the next round of infection. The surviving cells were reseeded in DMEM supplemented with 10% fetal bovine serum (FBS) and 1% penicillin/streptomycin solution and subjected to two more rounds of infection. Finally, the surviving cells were expanded to  $3.3 \times 10^7$  cells and were harvested to extract genomic DNA for deep-sequencing analysis.

**Illumina sequencing of sgRNAs in the genome-wide library and enriched mutants.** The genomic DNA of each sample was extracted using a quick-DNA midiprep plus kit (Zymo Research catalog no. D4075). The sgRNA-coding region was amplified by PCR using I-5 2 $\times$  high-fidelity master mix (Tsingke catalog no. TP001) in a reaction volume of 50  $\mu$ L. PCR products were mixed and purified with a MinElute PCR purification kit (Qiagen). All the purified PCR products were amplified by PCR using different bar-coded primers. All PCR products were pooled and purified with a MinElute PCR purification kit (Qiagen), followed by Illumina HiSeq  $\times$  Ten-PE150 next-generation sequencing. Mapped read counts were subsequently used as input for the MAGeCK analysis software package. Then, the top 0.5% ranked sgRNAs from the third and fourth EV71 challenge rounds were used to identify enriched targeted protein-coding genes. Kyoto Encyclopedia of Genes and Genomes (KEGG) enrichment analyses were performed in the Database for Annotation, Visualization and Integrated Discovery (DAVID) (<https://david.ncifcrf.gov/>) (87).

**Virus infection and titration.** HeLa cells were infected at a multiplicity of infection (MOI) of 0.1 with EV71 provided by Kailang Wu (State Key Laboratory of Virology, Wuhan University). The number of infectious virions was quantified using the median tissue culture infectious dose (TCID<sub>50</sub>) assay. The assay is performed by adding a serial dilution of the virus sample to cells in a 96-well plate. The type of cell was specifically selected to show a cytopathic effect (CPE), that is, morphological changes upon infection with the virus or cell death. For EV71, HeLa, RD, and Vero cells were able to be selected due to their susceptibility to EV71 infection. After an incubation period, the cells were inspected for CPE or cell death, and each well was classified as infected or not infected. The dilution at which 50% of the wells showed a

CPE was used to calculate the TCID<sub>50</sub> of the virus sample. The viral titers were determined as the TCID<sub>50</sub> per milliliter according to the Reed-Muench method.

**Clonal knockout and rescued cell line generation.** To generate the knockout cell lines, we first cloned the following sgRNA sequences into one vector system, lentiCRISPRv2 (one vector system, catalog no. 52961; Addgene), to target the indicated genes: 5'-TGTAGACCAGAGTATCGAGA-3' (SCARB2, [NM\\_005506.4](#)), 5'-ATCACCGGGTGGAGGCTTTA-3' (SLC35B2, [NM\\_178148.4](#)), 5'-TCCCTTACCCGAGTGCAGT-3' (B3GAT3, [NM\\_012200.4](#)), 5'-TGGAGGAGATCTCAAGTCT-3' (PAPSS1, [NM\\_005443.5](#)), 5'-TTCCGGCACAAGAGTTCG-3' (PAPSS2, [NM\\_004670.4](#)), 5'-GATAGAGCTCTACATTGAC-3' (TPST1, [NM\\_003596.4](#)), and 5'-CCCAGAGTCGAGCGGTCCA-3' (TPST2, [NM\\_001008566.3](#)). We then produced the corresponding lentivirus by transfecting HEK 293T cells with lentiCRISPRv2-target sgRNA, pMD2.G, and psPAX2. Following incubation for 48 h, the lentivirus supernatant was harvested, and cellular debris was filtered out using a 0.45- $\mu$ m Millipore filter. Next, HeLa or RD cells were transduced with the lentiviruses that expressed the sgRNAs. Mixed populations of infected cells were selected with 1  $\mu$ g/mL puromycin for 1 week 48 h posttransfection. Single-cell clones were screened and validated by immunoblotting analysis for protein expression using an available antibody, followed by Sanger sequencing using specific primers for PCR. The primers used are shown in Table S3. To generate reconstituted cell lines, we used another lentiviral vector, pCDH-CMV-IRES-MCS-SF-BLAST, to produce lentiviruses as described above. The KO clones were transduced with either a lentivirus expressing WT proteins or inactive proteins or an empty vector. The mixed cells were then selected with 10  $\mu$ g/mL blasticidin for 1 week.

**EV71 binding and internalization assay by RT-qPCR.** For the binding assay, EV71 was added to pre-cooled  $1.5 \times 10^5$  cells for 1 h at 4°C. After incubation, the supernatant was removed, and the cells were washed 3 times with phosphate-buffered saline (PBS) to remove unbound virions. The cells were harvested and then lysed with TRIzol reagent (Invitrogen), and after the addition of chloroform and phase separation, the total RNA was extracted. The viruses attached to the cell surface were determined by real-time quantitative PCR. The relative cell binding of EV71 viruses was calculated relative to GAPDH (glyceraldehyde-3-phosphate dehydrogenase) and normalized to control samples (wild-type cells). RT-qPCR analysis was performed on a Bio-Rad CFX96 Touch real-time PCR detection system. For the internalization assay, cells were first treated as for a binding assay and then incubated at 37°C with 5% CO<sub>2</sub> for 1 h. At 2 hpi, we removed the medium by aspiration, treated the cells with 1 mL of trypsin to detach them from the plate, and removed surface-bound virions that had not been internalized. We transferred the trypsinized cells to a microcentrifuge tube and pelleted the cells by centrifugation at  $500 \times g$  for 3 to 5 min at room temperature. We carefully removed the trypsin without disturbing the cell pellet. After three washes to remove PBS without disturbing the cell pellet, RNA was extracted for RT-qPCR analysis, as described above.

**Heparan sulfate surface staining.** Cells were detached with PBS and resuspended in fluorescence-activated cell sorter (FACS) buffer (1% bovine serum albumin [BSA] and 0.1% sodium azide [NaN<sub>3</sub>] in 1 $\times$  PBS). The cells were washed three times with FACS buffer by centrifugation at 4,000 rpm for 2 min at 4°C, followed by resuspension of the cell pellets. To stain for cell surface heparan sulfate, we incubated the cells for 1 h at 4°C with an anti-heparan sulfate mouse monoclonal antibody (10E4 epitope) (catalog no. 379225 [Amsbio]; 1:50 dilution). The cells were washed three times with FACS buffer as described above and subsequently stained with secondary goat anti-mouse IgM antibodies coupled to phycoerythrin (PE; catalog no. 550826 [BD Pharmingen]; 1:200 dilution). Then, the cells were resuspended in ice-cold PBS containing 3% BSA and 1% sodium azide and analyzed on a flow cytometer as soon as possible.

**RNA isolation and real-time quantitative PCR (RT-qPCR).** Total RNA was extracted from cells using TRIzol reagent (Invitrogen) and reverse transcribed using a PrimeScript RT reagent kit (catalog no. RR037B; TaKaRa). The RNA level was detected using 2 $\times$  universal SYBR green fast qPCR mix (catalog no. RM21203; ABclonal) in a CFX96 Touch real-time PCR detection system (Bio-Rad). The expression levels were calculated relative to GAPDH and normalized to control samples.

**Flow cytometry.** Cells were trypsinized and harvested by centrifugation at 4,000 rpm for 2 min at 4°C. Dil-labeled virions were added to the trypsinized cells and incubated for 1 h on ice. Unbound virus was washed off with cold PBS or fluorescence-activated cell sorting buffer (5 mM EDTA, 0.1% NaN<sub>3</sub>, and 1% fetal calf serum [FCS], in Dulbecco's PBS) three times. Cells were then resuspended in ice-cold PBS containing 3% BSA and 1% sodium azide and then analyzed on a CytoFLEX flow cytometer (Beckman) as soon as possible. Data analysis was performed using CytExpert software.

**Coimmunoprecipitation and Western blotting.** For the coimmunoprecipitation assay, the process was performed as follows. Briefly, the indicated plasmids were initially transfected into HEK293T cells. After incubation for 48 h, the cells were harvested, rinsed once with ice-cold phosphate-buffered saline (PBS; 137 mM NaCl, 2.7 mM KCl, 10 mM Na<sub>2</sub>HPO<sub>4</sub>, and 1.8 mM KH<sub>2</sub>PO<sub>4</sub>), and immediately lysed in lysis buffer (20 mM Tris-HCl [pH 7.4], 150 mM NaCl, 1 mM EDTA, 1% Triton X-100, 0.1% [wt/vol] SDS, and protease inhibitor cocktail) for 30 min on ice with gentle rocking every 10 min. Cell debris was removed by centrifugation at 13,000 rpm for 20 min at 4°C. Ten percent of the cell lysates were heat denatured in sample loading buffer (50 mM Tris-HCl [pH 6.8], 100 mM dithiothreitol [DTT], 2% SDS, 0.1% bromophenol blue, and 10% glycerol) and taken as the input. The remaining cell lysates were then incubated with either anti-Flag-conjugated agarose beads or anti-Myc-conjugated agarose beads (BioLegend) for 6 h at 4°C. After incubation, the beads were washed three or more times with lysis buffer and heat denatured in a sample loading buffer. After brief centrifugation, the proteins in the supernatants were separated by SDS-PAGE, followed by Western blotting analysis. For Western blotting, cell lysates were cleared by centrifugation at 13,000 rpm for 20 min at 4°C and then heated at 95°C for 10 min, except for the detection of CCR5 and SLC35B2 (high temperatures cause the aggregation of multipass membrane proteins; thus, they must be incubated at 37°C for 30 min). The protein samples from various cell preparations and rainbow molecular weight markers were separated by SDS-PAGE and then electrotransferred onto

nitrocellulose membranes, followed by blocking with 5% nonfat milk and probing with the indicated antibodies. The blots were incubated with Immobilon Western HRP substrate (Millipore) and visualized by using the chemiluminescence imaging system (Fujifilm). The following primary antibodies were used for Western blotting: mouse anti-VP1 (1:2,000; AbMax), mouse anti-HN (1:1,000; Abcam), mouse anti-ENV (1:2,000; BioFront), mouse anti-GAPDH (1:5,000; ABclonal), mouse anti-alpha-tubulin (1:5,000; ABclonal), rabbit anti-DYKDDDDK tag (1:5,000; MBL), rabbit anti-Myc tag (1:5,000; MBL), rabbit anti-HA tag (1:5,000; MBL), rabbit anti-LIMP2 (1:2,000; Abcam), rabbit anti-B3GAT3 (1:2,000; Abcam), rabbit anti-PAPSS1 (1:2,000; Abcam), and rabbit anti-PAPSS2 (1:2,000; Abcam).

**Immunofluorescence analysis.** HeLa cells were cultured on coverslips in 24-well plates overnight. After transfection and/or infection, cells were harvested at the indicated times. Cells were fixed with 4% paraformaldehyde (PFA) for 20 min and permeabilized with 0.2% Triton X-100 for 20 min at room temperature. After being blocked with 3% bovine serum albumin (BSA) for 30 min, the cells were incubated with primary antibodies diluted in 1% BSA at 4°C overnight, and secondary antibodies were diluted in 1% BSA and incubated with the cells at room temperature for another 1 h. The cells were examined using a Leica confocal microscope after staining with 1 mg/mL 4',6-diamidino-2-phenylindole (DAPI) in PBS. The primary antibodies used were as follows: rabbit anti-TGN46 (1:200; Abcam), mouse anti-HA tag (1:2,000; Sigma), mouse anti-Flag tag (1:1,000; Sigma), and mouse anti-Myc tag (1:200; Santa Cruz). The secondary antibodies used were as follows: Alexa Fluor 488 donkey anti-rabbit IgG (1:1,000; Invitrogen) and Alexa Fluor 594 donkey anti-mouse IgG (1:1,000; Invitrogen).

**Metabolic labeling with sulfate.** Cells were seeded into six-well plates until they reached ~70% confluence, and 100  $\mu$ Ci/mL [<sup>35</sup>S]O<sub>4</sub> (sulfur-35 radionuclide; PerkinElmer) or 33  $\mu$ Ci/mL [<sup>35</sup>S]methionine/[<sup>35</sup>S]cysteine (EasyTag Express <sup>35</sup>S protein labeling mix; PerkinElmer) was added to methionine- and cysteine-free DMEM (Sigma) in each well. Then, the cells were incubated for ~36 h at 37°C with 5% CO<sub>2</sub>. The labeled cells were harvested and lysed in lysis buffer on ice. The samples were resolved on 12% SDS-PAGE gels. After the gels were dried, filmless autoradiography was performed using a Cyclone plus storage phosphor system (PerkinElmer). Reusable storage phosphor screens capture and store the radioactivity of samples to which they are exposed, as with the film in common film cassettes. The screens were scanned using a laser focused to less than 50  $\mu$ m, and the latent image was detected by unique confocal optics to create a high-resolution digitized image with quantitative data in the form of an image file. The image was displayed on the screen for analysis with the OptiQuant software.

**Cell proliferation assay.** According to the guidelines, the cell proliferation ability of the knockout cell lines was monitored using a cell counting kit/CCK-8 cell proliferation/viability assay kit (catalog no. ZP328; Zomanbio).

**Cytotoxicity analysis.** The cytotoxicity of heparin, chondroitin sulfate, and sodium chlorate was determined using a cell counting kit/CCK-8 cell proliferation/viability assay kit (catalog no. ZP328). Briefly, various concentrations of these compounds were added to overnight-cultured HeLa or RD cells; then, they were incubated overnight or for a specified duration. Ten microliters of the CCK-8 cell proliferation assay reagent was then added to each well. The plate was then analyzed at an absorbance of 450 nm after 2 h of incubation at 37°C.

**Statistical analysis.** Statistical analysis was performed with GraphPad Prism version 6.0. An unpaired two-tailed Student *t* test was used to determine statistical significance, and *P* values of <0.05, <0.01, <0.001, and <0.0001 were considered significant and are denoted with one, two, three, and four asterisks, respectively. A *P* value of >0.05 was considered statistically nonsignificant and is denoted as “ns.”

## SUPPLEMENTAL MATERIAL

Supplemental material is available online only.

**SUPPLEMENTAL FILE 1**, XLSX file, 2 MB.

**SUPPLEMENTAL FILE 2**, XLSX file, 7.9 MB.

**SUPPLEMENTAL FILE 3**, XLSX file, 0.01 MB.

**SUPPLEMENTAL FILE 4**, PDF file, 0.02 MB.

## ACKNOWLEDGMENTS

We are grateful to Kailang Wu (Wuhan University, China) for EV71 and Ke Lan (Wuhan University, China) for the streptomycin-Flag-tagged pCDH-CMV-IRES-MCS-SF-BLAST vector. We thank Feng Zhang (MIT) for kindly sharing the human GeCKO library (Addgene).

This work was supported by grants from the National Key R&D Program of China (2021YFC2300702 and 2021YFC2300200), the National Natural Science Foundation of China (82130064, 81825015, and 81871650).

## REFERENCES

- McMinn PC. 2002. An overview of the evolution of enterovirus 71 and its clinical and public health significance. *FEMS Microbiol Rev* 26:91–107. <https://doi.org/10.1111/j.1574-6976.2002.tb00601.x>.
- Wang SM, Liu CC, Tseng HW, Wang JR, Huang CC, Chen YJ, Yang YJ, Lin SJ, Yeh TF. 1999. Clinical spectrum of enterovirus 71 infection in children in southern Taiwan, with an emphasis on neurological

- complications. *Clin Infect Dis* 29:184–190. <https://doi.org/10.1086/520149>.
3. Ryu WS, Kang B, Hong J, Hwang S, Kim A, Kim J, Cheon DS. 2010. Enterovirus 71 infection with central nervous system involvement, South Korea. *Emerg Infect Dis* 16:1764–1766. <https://doi.org/10.3201/eid1611.100104>.
  4. Yamayoshi S, Yamashita Y, Li J, Hanagata N, Minowa T, Takemura T, Koike S. 2009. Scavenger receptor B2 is a cellular receptor for enterovirus 71. *Nat Med* 15:798–801. <https://doi.org/10.1038/nm.1992>.
  5. Nishimura Y, Shimojima M, Tano Y, Miyamura T, Wakita T, Shimizu H. 2009. Human P-selectin glycoprotein ligand-1 is a functional receptor for enterovirus 71. *Nat Med* 15:794–797. <https://doi.org/10.1038/nm.1961>.
  6. Su PY, Wang YF, Huang SW, Lo YC, Wang YH, Wu SR, Shieh DB, Chen SH, Wang JR, Lai MD, Chang CF. 2015. Cell surface nucleolin facilitates enterovirus 71 binding and infection. *J Virol* 89:4527–4538. <https://doi.org/10.1128/JVI.03498-14>.
  7. Yang SL, Chou YT, Wu CN, Ho MS. 2011. Annexin II binds to capsid protein VP1 of enterovirus 71 and enhances viral infectivity. *J Virol* 85:11809–11820. <https://doi.org/10.1128/JVI.00297-11>.
  8. Du N, Cong H, Tian H, Zhang H, Zhang W, Song L, Tien P. 2014. Cell surface vimentin is an attachment receptor for enterovirus 71. *J Virol* 88:5816–5833. <https://doi.org/10.1128/JVI.03826-13>.
  9. Tan CW, Poh CL, Sam IC, Chan YF. 2013. Enterovirus 71 uses cell surface heparan sulfate glycosaminoglycan as an attachment receptor. *J Virol* 87:611–620. <https://doi.org/10.1128/JVI.02226-12>.
  10. Yang B, Chuang H, Yang KD. 2009. Sialylated glycans as receptor and inhibitor of enterovirus 71 infection to DLD-1 intestinal cells. *Virology* 397:11–17. <https://doi.org/10.1016/j.virol.2010.09.025>.
  11. Ren XX, Ma L, Liu QW, Li C, Huang Z, Wu L, Xiong SD, Wang JH, Wang HB. 2014. The molecule of DC-SIGN captures enterovirus 71 and confers dendritic cell-mediated viral trans-infection. *Virology* 461:47–54. <https://doi.org/10.1016/j.virol.2014.02.012>.
  12. Too IHK, Bonne I, Tan EL, Chu JJH, Alonso S. 2018. Prohibitin plays a critical role in enterovirus 71 neuropathogenesis. *PLoS Pathog* 14:e1006778. <https://doi.org/10.1371/journal.ppat.1006778>.
  13. He QQ, Ren S, Xia ZC, Cheng ZK, Peng NF, Zhu Y. 2018. Fibronectin facilitates enterovirus 71 infection by mediating viral entry. *J Virol* 92:e02251-17. <https://doi.org/10.1128/JVI.02251-17>.
  14. Fujii K, Nagata N, Sato Y, Ong KC, Wong KT, Yamayoshi S, Shimanuki M, Shitara H, Taya C, Koike S. 2013. Transgenic mouse model for the study of enterovirus 71 neuropathogenesis. *Proc Natl Acad Sci U S A* 110:14753–14758. <https://doi.org/10.1073/pnas.1217563110>.
  15. Lewandrowski U, Moebius J, Walter U, Sickmann A. 2006. Elucidation of N-glycosylation sites on human platelet proteins: a glycoproteomic approach. *Mol Cell Proteomics* 5:226–233. <https://doi.org/10.1074/mcp.M500324-MCP200>.
  16. Su PY, Liu YT, Chang HY, Huang SW, Wang YF, Yu CK, Wang JR, Chang CF. 2012. Cell surface sialylation affects binding of enterovirus 71 to rhabdomyosarcoma and neuroblastoma cells. *BMC Microbiol* 12:162. <https://doi.org/10.1186/1471-2180-12-162>.
  17. Hussain KM, Leong KL, Ng MM, Chu JJ. 2011. The essential role of clathrin-mediated endocytosis in the infectious entry of human enterovirus 71. *J Biol Chem* 286:309–321. <https://doi.org/10.1074/jbc.M110.168468>.
  18. Somers WS, Tang J, Shaw GD, Camphausen RT. 2000. Insights into the molecular basis of leukocyte tethering and rolling revealed by structures of P- and E-selectin bound to SLe(X) and PSGL-1. *Cell* 103:467–479. [https://doi.org/10.1016/s0092-8674\(00\)00138-0](https://doi.org/10.1016/s0092-8674(00)00138-0).
  19. Nishimura Y, Wakita T, Shimizu H. 2010. Tyrosine sulfation of the amino terminus of PSGL-1 is critical for enterovirus 71 infection. *PLoS Pathog* 6:e1001174. <https://doi.org/10.1371/journal.ppat.1001174>.
  20. Miyamura K, Nishimura Y, Abo M, Wakita T, Shimizu H. 2011. Adaptive mutations in the genomes of enterovirus 71 strains following infection of mouse cells expressing human P-selectin glycoprotein ligand-1. *J Gen Virol* 92:287–291. <https://doi.org/10.1099/vir.0.022418-0>.
  21. Nishimura Y, Lee H, Hafenstein S, Kataoka C, Wakita T, Bergelson JM, Shimizu H. 2013. Enterovirus 71 binding to PSGL-1 on leukocytes: VP1-145 acts as a molecular switch to control receptor interaction. *PLoS Pathog* 9:e1003511. <https://doi.org/10.1371/journal.ppat.1003511>.
  22. Busse-Wicher M, Wicher KB, Kusche-Gullberg M. 2014. The exostosin family: proteins with many functions. *Matrix Biol* 35:25–33. <https://doi.org/10.1016/j.matbio.2013.10.001>.
  23. Rabenstein DL. 2002. Heparin and heparan sulfate: structure and function. *Nat Prod Rep* 19:312–331. <https://doi.org/10.1039/b100916h>.
  24. Shriver Z, Capila I, Venkataraman G, Sasisekharan R. 2012. Heparin and heparan sulfate: analyzing structure and microheterogeneity. *Handb Exp Pharmacol* 2012:159–176. [https://doi.org/10.1007/978-3-642-23056-1\\_8](https://doi.org/10.1007/978-3-642-23056-1_8).
  25. Cagno V, Tseligka ED, Jones ST, Tapparel C. 2019. Heparan sulfate proteoglycans and viral attachment: true receptors or adaptation bias? *Viruses* 11:596. <https://doi.org/10.3390/v11070596>.
  26. Artpradit C, Robinson LN, Gavrilov BK, Rurak TT, Ruchirawat M, Sasisekharan R. 2013. Recognition of heparan sulfate by clinical strains of dengue virus serotype 1 using recombinant subviral particles. *Virus Res* 176:69–77. <https://doi.org/10.1016/j.virusres.2013.04.017>.
  27. Shukla D, Liu J, Blaiklock P, Shworak NW, Bai X, Esko JD, Cohen GH, Eisenberg RJ, Rosenberg RD, Spear PG. 1999. A novel role for 3-O-sulfated heparan sulfate in herpes simplex virus 1 entry. *Cell* 99:13–22. [https://doi.org/10.1016/s0092-8674\(00\)80058-6](https://doi.org/10.1016/s0092-8674(00)80058-6).
  28. Giroglou T, Florin L, Schäfer F, Streeck RE, Sapp M. 2001. Human papillomavirus infection requires cell surface heparan sulfate. *J Virol* 75:1565–1570. <https://doi.org/10.1128/JVI.75.3.1565-1570.2001>.
  29. Sa-Carvalho D, Rieder E, Baxt B, Rodarte R, Tanuri A, Mason PW. 1997. Tissue culture adaptation of foot-and-mouth disease virus selects viruses that bind to heparin and are attenuated in cattle. *J Virol* 71:5115–5123. <https://doi.org/10.1128/JVI.71.7.5115-5123.1997>.
  30. Wang Y, Pfeiffer JK. 2016. Emergence of a large-plaque variant in mice infected with coxsackievirus B3. *mBio* 7:e00119-16. <https://doi.org/10.1128/mBio.00119-16>.
  31. Bochkov YA, Watters K, Basnet S, Sijapati S, Hill M, Palmenberg AC, Gern JE. 2016. Mutations in VP1 and 3A proteins improve binding and replication of rhinovirus C15 in HeLa-E8 cells. *Virology* 499:350–360. <https://doi.org/10.1016/j.virol.2016.09.025>.
  32. Khan AG, Pickl-Herk A, Gajdzik L, Marlovits TC, Fuchs R, Blaas D. 2011. Entry of a heparan sulphate-binding HRV8 variant strictly depends on dynamin but not on clathrin, caveolin, and flotillin. *Virology* 412:55–67. <https://doi.org/10.1016/j.virol.2010.12.042>.
  33. Tseligka ED, Sobo K, Stoppini L, Cagno V, Abdul F, Piuze I, Meylan P, Huang S, Constant S, Tapparel C. 2018. A VP1 mutation acquired during an enterovirus 71 disseminated infection confers heparan sulfate binding ability and modulates ex vivo tropism. *PLoS Pathog* 14:e1007190. <https://doi.org/10.1371/journal.ppat.1007190>.
  34. Cordey S, Petty TJ, Schibler M, Martinez Y, Gerlach D, van Belle S, Turin L, Zdobnov E, Kaiser L, Tapparel C. 2012. Identification of site-specific adaptations conferring increased neural cell tropism during human enterovirus 71 infection. *PLoS Pathog* 8:e1002826. <https://doi.org/10.1371/journal.ppat.1002826>.
  35. Johnson SM, McNally BA, Ioannidis I, Flano E, Teng MN, Oomens AG, Walsh EE, Peeples ME. 2015. Respiratory syncytial virus uses CX3CR1 as a receptor on primary human airway epithelial cultures. *PLoS Pathog* 11:e1005318. <https://doi.org/10.1371/journal.ppat.1005318>.
  36. Cagno V, Donalisio M, Civra A, Volante M, Vecelli E, Oreste P, Rusnati M, Lembo D. 2014. Highly sulfated K5 Escherichia coli polysaccharide derivatives inhibit respiratory syncytial virus infectivity in cell lines and human tracheal-bronchial histocultures. *Antimicrob Agents Chemother* 58:4782–4794. <https://doi.org/10.1128/AAC.02594-14>.
  37. Donalisio M, Rusnati M, Cagno V, Civra A, Bugatti A, Giuliani A, Pirri G, Volante M, Papotti M, Landolfo S, Lembo D. 2012. Inhibition of human respiratory syncytial virus infectivity by a dendrimeric heparan sulfate-binding peptide. *Antimicrob Agents Chemother* 56:5278–5288. <https://doi.org/10.1128/AAC.00771-12>.
  38. Bose S, Banerjee AK. 2002. Role of heparan sulfate in human parainfluenza virus type 3 infection. *Virology* 298:73–83. <https://doi.org/10.1006/viro.2002.1484>.
  39. Zhang L, Bukreyev A, Thompson CI, Watson B, Peeples ME, Collins PL, Pickles RJ. 2005. Infection of ciliated cells by human parainfluenza virus type 3 in an in vitro model of human airway epithelium. *J Virol* 79:1113–1124. <https://doi.org/10.1128/JVI.79.2.1113-1124.2005>.
  40. Kim SY, Zhao J, Liu X, Fraser K, Lin L, Zhang X, Zhang F, Dordick JS, Linhardt RJ. 2017. Interaction of Zika virus envelope protein with glycosaminoglycans. *Biochemistry* 56:1151–1162. <https://doi.org/10.1021/acs.biochem.6b01056>.
  41. Ghezzi S, Cooper L, Rubio A, Paganì I, Capobianchi MR, Ippolito G, Pelletier J, Meneghetti MCZ, Lima MA, Skidmore MA, Broccoli V, Yates EA, Vicenzi E. 2017. Heparin prevents Zika virus induced-cytopathic effects in human neural progenitor cells. *Antiviral Res* 140:13–17. <https://doi.org/10.1016/j.antiviral.2016.12.023>.
  42. Gao H, Lin Y, He J, Zhou S, Liang M, Huang C, Li X, Liu C, Zhang P. 2019. Role of heparan sulfate in the Zika virus entry, replication, and cell death. *Virology* 529:91–100. <https://doi.org/10.1016/j.virol.2019.01.019>.

43. Kobayashi K, Koike S. 2020. Cellular receptors for enterovirus A71. *J Biomed Sci* 27:23. <https://doi.org/10.1186/s12929-020-0615-9>.
44. Baeuerle PA, Huttner WB. 1987. Tyrosine sulfation is a trans-Golgi-specific protein modification. *J Cell Biol* 105:2655–2664. <https://doi.org/10.1083/jcb.105.6.2655>.
45. Vos JP, Lopes-Cardozo M, Gadella BM. 1994. Metabolic and functional aspects of sulfogalactolipids. *Biochim Biophys Acta* 1211:125–149. [https://doi.org/10.1016/0005-2760\(94\)90262-3](https://doi.org/10.1016/0005-2760(94)90262-3).
46. Yin Y, Wang A, Feng L, Wang Y, Zhang H, Zhang I, Bany BM, Ma L. 2018. Heparan sulfate proteoglycan sulfation regulates uterine differentiation and signaling during embryo implantation. *Endocrinology* 159:2459–2472. <https://doi.org/10.1210/en.2018-00105>.
47. Venkatachalam KV. 2003. Human 3'-phosphoadenosine 5'-phosphosulfate (PAPS) synthase: biochemistry, molecular biology and genetic deficiency. *IUBMB Life* 55:1–11. <https://doi.org/10.1080/1521654031000072148>.
48. Besset S, Vincourt JB, Amalric F, Girard JP. 2000. Nuclear localization of PAPS synthetase 1: a sulfate activation pathway in the nucleus of eukaryotic cells. *FASEB J* 14:345–354. <https://doi.org/10.1096/fasebj.14.2.345>.
49. Kamiyama S, Suda T, Ueda R, Suzuki M, Okubo R, Kikuchi N, Chiba Y, Goto S, Toyoda H, Saigo K, Watanabe M, Narimatsu H, Jigami Y, Nishihara S. 2003. Molecular cloning and identification of 3'-phosphoadenosine 5'-phosphosulfate transporter. *J Biol Chem* 278:25958–25963. <https://doi.org/10.1074/jbc.M302439200>.
50. Bowman KG, Bertozzi CR. 1999. Carbohydrate sulfotransferases: mediators of extracellular communication. *Chem Biol* 6:R9–R22. [https://doi.org/10.1016/S1074-5521\(99\)80014-3](https://doi.org/10.1016/S1074-5521(99)80014-3).
51. Westmuckett AD, Thacker KM, Moore KL. 2011. Tyrosine sulfation of native mouse Psgl-1 is required for optimal leukocyte rolling on P-selectin in vivo. *PLoS One* 6:e20406. <https://doi.org/10.1371/journal.pone.0020406>.
52. Farzan M, Mirzabekov T, Kolchinsky P, Wyatt R, Cayabyab M, Gerard NP, Gerard C, Sodroski J, Choe H. 1999. Tyrosine sulfation of the amino terminus of CCR5 facilitates HIV-1 entry. *Cell* 96:667–676. [https://doi.org/10.1016/S0092-8674\(00\)80577-2](https://doi.org/10.1016/S0092-8674(00)80577-2).
53. Leyte A, van Schijndel HB, Niehrs C, Huttner WB, Verbeet MP, Mertens K, van Mourik JA. 1991. Sulfation of Tyr1680 of human blood coagulation factor VIII is essential for the interaction of factor VIII with von Willebrand factor. *J Biol Chem* 266:740–746. [https://doi.org/10.1016/S0021-9258\(17\)35234-1](https://doi.org/10.1016/S0021-9258(17)35234-1).
54. Wu KX, Phuektes P, Kumar P, Goh GY, Moreau D, Chow VT, Bard F, Chu JJ. 2016. Human genome-wide RNAi screen reveals host factors required for enterovirus 71 replication. *Nat Commun* 7:13150. <https://doi.org/10.1038/ncomms13150>.
55. Yeung ML, Jia L, Yip CCY, Chan JFW, Teng JLL, Chan KH, Cai JP, Zhang C, Zhang AJ, Wong WM, Kok KH, Lau SKP, Woo PCY, Lo JYC, Jin DY, Shih SR, Yuen KY. 2018. Human tryptophanyl-tRNA synthetase is an IFN- $\gamma$ -inducible entry factor for Enterovirus. *J Clin Invest* 128:5163–5177. <https://doi.org/10.1172/JCI99411>.
56. Housden BE, Perrimon N. 2016. Comparing CRISPR and RNAi-based screening technologies. *Nat Biotechnol* 34:621–623. <https://doi.org/10.1038/nbt.3599>.
57. Morgens DW, Deans RM, Li A, Bassik MC. 2016. Systematic comparison of CRISPR/Cas9 and RNAi screens for essential genes. *Nat Biotechnol* 34:634–636. <https://doi.org/10.1038/nbt.3567>.
58. Zhang R, Miner JJ, Gorman MJ, Rausch K, Ramage H, White JP, Zuiani A, Zhang P, Fernandez E, Zhang Q, Dowd KA, Pierson TC, Cherry S, Diamond MS. 2016. A CRISPR screen defines a signal peptide processing pathway required by flaviviruses. *Nature* 535:164–168. <https://doi.org/10.1038/nature18625>.
59. Richardson RB, Ohlson MB, Eitson JL, Kumar A, McDougal MB, Boys IN, Mar KB, De La Cruz-Rivera PC, Douglas C, Konopka G, Xing C, Schoggins JW. 2018. A CRISPR screen identifies IFI6 as an ER-resident interferon effector that blocks flavivirus replication. *Nat Microbiol* 3:1214–1223. <https://doi.org/10.1038/s41564-018-0244-1>.
60. Li Y, Muffat J, Omer Javed A, Keys HR, Lungjangwa T, Bosch I, Khan M, Virgilio MC, Gehrke L, Sabatini DM, Jaenisch R. 2019. Genome-wide CRISPR screen for Zika virus resistance in human neural cells. *Proc Natl Acad Sci U S A* 116:9527–9532. <https://doi.org/10.1073/pnas.1900867116>.
61. Hoffmann HH, Schneider WM, Rozen-Gagnon K, Miles LA, Schuster F, Razoooky B, Jacobson E, Wu X, Yi S, Rudin CM, MacDonald MR, McMullan LK, Poirier JT, Rice CM. 2021. TMEM41B is a pan-flavivirus host factor. *Cell* 184:133–148.e20. <https://doi.org/10.1016/j.cell.2020.12.005>.
62. Shalem O, Sanjana NE, Hartenian E, Shi X, Scott DA, Mikkelsen T, Heckl D, Ebert BL, Root DE, Doench JG, Zhang F. 2014. Genome-scale CRISPR-Cas9 knockout screening in human cells. *Science* 343:84–87. <https://doi.org/10.1126/science.1247005>.
63. Han J, Perez JT, Chen C, Li Y, Benitez A, Kandasamy M, Lee Y, Andrade J, tenOever B, Manicassamy B. 2018. Genome-wide CRISPR/Cas9 screen identifies host factors essential for influenza virus replication. *Cell Rep* 23:596–607. <https://doi.org/10.1016/j.celrep.2018.03.045>.
64. Joung J, Konermann S, Gootenberg JS, Abudayyeh OO, Platt RJ, Brigham MD, Sanjana NE, Zhang F. 2017. Genome-scale CRISPR-Cas9 knockout and transcriptional activation screening. *Nat Protoc* 12:828–863. <https://doi.org/10.1038/nprot.2017.016>.
65. Park RJ, Wang T, Koundakjian D, Hultquist JF, Lamothe-Molina P, Monel B, Schumann K, Yu H, Krupczak KM, Garcia-Beltran W, Piechocka-Trocha A, Krogan NJ, Marson A, Sabatini DM, Lander ES, Hacohen N, Walker BD. 2017. A genome-wide CRISPR screen identifies a restricted set of HIV host dependency factors. *Nat Genet* 49:193–203. <https://doi.org/10.1038/ng.3741>.
66. Blondel CJ, Park JS, Hubbard TP, Pacheco AR, Kuehl CJ, Walsh MJ, Davis BM, Gewurz BE, Doench JG, Waldor MK. 2016. CRISPR/Cas9 screens reveal requirements for host cell sulfation and fucosylation in bacterial type III secretion system-mediated cytotoxicity. *Cell Host Microbe* 20:226–237. <https://doi.org/10.1016/j.chom.2016.06.010>.
67. Rosmarin DM, Carette JE, Olive AJ, Starnbach MN, Brummelkamp TR, Ploegh HL. 2012. Attachment of Chlamydia trachomatis L2 to host cells requires sulfation. *Proc Natl Acad Sci U S A* 109:10059–10064. <https://doi.org/10.1073/pnas.1120244109>.
68. Berry GE, Tse LV. 2017. Virus binding and internalization assay for adeno-associated virus. *Bio Protoc* 7:e2110. <https://doi.org/10.21769/BioProtoc.2110>.
69. Reczek D, Schwake M, Schröder J, Hughes H, Blanz J, Jin X, Brondyk W, Van Patten S, Edmunds T, Saftig P. 2007. LIMP-2 is a receptor for lysosomal mannose-6-phosphate-independent targeting of beta-glucocerebrosidase. *Cell* 131:770–783. <https://doi.org/10.1016/j.cell.2007.10.018>.
70. Yamayoshi S, Koike S. 2011. Identification of a human SCARB2 region that is important for enterovirus 71 binding and infection. *J Virol* 85:4937–4946. <https://doi.org/10.1128/JVI.02358-10>.
71. Lin YW, Lin HY, Tsou YL, Chitra E, Hsiao KN, Shao HY, Liu CC, Sia C, Chong P, Chow YH. 2012. Human SCARB2-mediated entry and endocytosis of EV71. *PLoS One* 7:e30507. <https://doi.org/10.1371/journal.pone.0030507>.
72. Dang M, Wang X, Wang Q, Wang Y, Lin J, Sun Y, Li X, Zhang L, Lou Z, Wang J, Rao Z. 2014. Molecular mechanism of SCARB2-mediated attachment and uncoating of EV71. *Protein Cell* 5:692–703. <https://doi.org/10.1007/s13238-014-0087-3>.
73. Yamayoshi S, Ohka S, Fujii K, Koike S. 2013. Functional comparison of SCARB2 and PSLG1 as receptors for enterovirus 71. *J Virol* 87:3335–3347. <https://doi.org/10.1128/JVI.02070-12>.
74. Schwake M, Schröder B, Saftig P. 2013. Lysosomal membrane proteins and their central role in physiology. *Traffic* 14:739–748. <https://doi.org/10.1111/tra.12056>.
75. Hallak LK, Spillmann D, Collins PL, Peeples ME. 2000. Glycosaminoglycan sulfation requirements for respiratory syncytial virus infection. *J Virol* 74:10508–10513. <https://doi.org/10.1128/jvi.74.22.10508-10513.2000>.
76. Seibert C, Cadene M, Sanfiz A, Chait BT, Sakmar TP. 2002. Tyrosine sulfation of CCR5 N-terminal peptide by tyrosylprotein sulfotransferases 1 and 2 follows a discrete pattern and temporal sequence. *Proc Natl Acad Sci U S A* 99:11031–11036. <https://doi.org/10.1073/pnas.172380899>.
77. Liu MC, Yu S, Sy J, Redman CM, Lipmann F. 1985. Tyrosine sulfation of proteins from the human hepatoma cell line HepG2. *Proc Natl Acad Sci U S A* 82:7160–7164. <https://doi.org/10.1073/pnas.82.21.7160>.
78. Tan CW, Sam IC, Lee VS, Wong HV, Chan YF. 2017. VP1 residues around the five-fold axis of enterovirus A71 mediate heparan sulfate interaction. *Virology* 501:79–87. <https://doi.org/10.1016/j.virol.2016.11.009>.
79. Chang CK, Wu SR, Chen YC, Lee KJ, Chung NH, Lu YJ, Yu SL, Liu CC, Chow YH. 2018. Mutations in VP1 and 5'-UTR affect enterovirus 71 virulence. *Sci Rep* 8:6688. <https://doi.org/10.1038/s41598-018-25091-7>.
80. Kobayashi K, Sudaka Y, Takashino A, Imura A, Fujii K, Koike S. 2018. Amino acid variation at VP1-145 of enterovirus 71 determines attachment receptor usage and neurovirulence in human scavenger receptor B2 transgenic mice. *J Virol* 92:e00681-18. <https://doi.org/10.1128/JVI.00681-18>.
81. Fujii K, Sudaka Y, Takashino A, Kobayashi K, Kataoka C, Suzuki T, Iwata-Yoshikawa N, Kotani O, Ami Y, Shimizu H, Nagata N, Mizuta K, Matsuzaki Y, Koike S. 2018. VP1 amino acid residue 145 of enterovirus 71 is a key residue for its receptor attachment and resistance to neutralizing antibody during cynomolgus monkey infection. *J Virol* 92:e00682-18. <https://doi.org/10.1128/JVI.00682-18>.
82. Tee HK, Tan CW, Yogarajah T, Lee MHP, Chai HJ, Hanapi NA, Yusof SR, Ong KC, Lee VS, Sam IC, Chan YF. 2019. Electrostatic interactions at the five-fold axis alter heparin-binding phenotype and drive enterovirus A71

- virulence in mice. *PLoS Pathog* 15:e1007863. <https://doi.org/10.1371/journal.ppat.1007863>.
83. Kobayashi K, Mizuta K, Koike S. 2020. Heparan sulfate attachment receptor is a major selection factor for attenuated enterovirus 71 mutants during cell culture adaptation. *PLoS Pathog* 16:e1008428. <https://doi.org/10.1371/journal.ppat.1008428>.
84. Clausen TM, Sandoval DR, Spliid CB, Pihl J, Perrett HR, Painter CD, Narayanan A, Majowicz SA, Kwong EM, McVicar RN, Thacker BE, Glass CA, Yang Z, Torres JL, Golden GJ, Bartels PL, Porell RN, Garretson AF, Laubach L, Feldman J, Yin X, Pu Y, Hauser BM, Caradonna TM, Kellman BP, Martino C, Gordts P, Chanda SK, Schmidt AG, Godula K, Leibel SL, Jose J, Corbett KD, Ward AB, Carlin AF, Esko JD. 2020. SARS-CoV-2 infection depends on cellular heparan sulfate and ACE2. *Cell* 183:1043–1057.e15. <https://doi.org/10.1016/j.cell.2020.09.033>.
85. Schneider WM, Luna JM, Hoffmann HH, Sánchez-Rivera FJ, Leal AA, Ashbrook AW, Le Pen J, Ricardo-Lax I, Michailidis E, Peace A, Stenzel AF, Lowe SW, MacDonald MR, Rice CM, Poirier JT. 2021. Genome-scale identification of SARS-CoV-2 and pan-coronavirus host factor networks. *Cell* 184:120–132.e14. <https://doi.org/10.1016/j.cell.2020.12.006>.
86. Wang R, Simoneau CR, Kulsuptrakul J, Bouhaddou M, Travisano KA, Hayashi JM, Carlson-Stevermer J, Zengel JR, Richards CM, Fozouni P, Oki J, Rodriguez L, Joehnk B, Walcott K, Holden K, Sil A, Carette JE, Krogan NJ, Ott M, Puschnik AS. 2021. Genetic screens identify host factors for SARS-CoV-2 and common cold coronaviruses. *Cell* 184:106–119.e14. <https://doi.org/10.1016/j.cell.2020.12.004>.
87. Dennis G, Jr, Sherman BT, Hosack DA, Yang J, Gao W, Lane HC, Lempicki RA. 2003. DAVID: database for annotation, visualization, and integrated discovery. *Genome Biol* 4:P3. <https://doi.org/10.1186/gb-2003-4-5-p3>.